

# Exploiting Low-Rank Structure in Max- $K$ -Cut Problems

Ria Stevens  
Rice University  
ria.stevens@rice.edu

Fangshuo Liao  
Rice University  
fangshuo.liao@rice.edu

Barbara Su  
Rice University  
barbara.su@rice.edu

Jianqiang Li  
Rice University  
jl567@rice.edu

Anastasios Kyrillidis  
Rice University  
anastasios@rice.edu

## Abstract

We approach the MAX-3-CUT problem through the lens of maximizing complex-valued quadratic forms and demonstrate that low-rank structure in the objective matrix can be exploited, leading to alternative algorithms to classical semidefinite programming (SDP) relaxations and heuristic techniques. We propose an algorithm for maximizing these quadratic forms over a domain of size  $K$  that enumerates and evaluates a set of  $\mathcal{O}(n^{2r-1})$  candidate solutions, where  $n$  is the dimension of the matrix and  $r$  represents the rank of an approximation of the objective. We prove that this candidate set is guaranteed to include the exact maximizer when  $K = 3$  (corresponding to MAX-3-CUT) and the objective is low-rank, and provide approximation guarantees when the objective is a perturbation of a low-rank matrix. This construction results in a family of novel, inherently parallelizable and theoretically-motivated algorithms for MAX-3-CUT. Extensive experimental results demonstrate that our approach achieves performance comparable to existing algorithms across a wide range of graphs, while being highly scalable.

## 1 Introduction

Maximum Cut (MAX-2-CUT) and Maximum 3-Cut (MAX-3-CUT) are fundamental problems in combinatorial optimization with applications in VLSI design, clustering, network analysis [FHL<sup>+</sup>19, BP21]. Recently, these problems have also been extensively used as target problems to study quantum computing [GD24, FGG14]. In MAX-2-CUT, we seek to partition a graph’s vertices into two sets such that the sum of weights of edges crossing the partition is maximized. Mathematically, this translates to the problem:

$$\text{OPT-Q}^* := \max_{\mathbf{z} \in \{\pm 1\}^n} \mathbf{z}^\top \mathbf{Q}^* \mathbf{z}, \quad (1)$$

where  $\mathbf{Q}^*$  is a symmetric data matrix in  $\mathbb{R}^{n \times n}$  (i.e., the positive semi-definite (PSD) Laplacian of a graph) and  $\mathbf{z} \in \{\pm 1\}^n$  is the discrete variable vector (i.e., the assignment vector to different sets in MAX-2-CUT). More problem instances can be written as in (1), such as the maximum colored cut problem [Sot15], but we focus on maximum cut instances in this work.

Specifically, we study MAX-3-CUT, the first generalization of the MAX-2-CUT problem beyond two sets [CRS98, FJ97, New18, Vit81, dKPW04, GW01]. In MAX-3-CUT, we seek to partition nodes into 3 sets, maximizing the total weight of the edges between nodes in different sets. Existing algorithms for MAX-3-CUT work in both real-space [FJ97] as well as in complex-space [GW01]. The more general MAX- $K$ -CUT problem has been well-studied in the real case [FJ97], while extensions to any  $K > 3$  in the complex case are not yet fully understood.

Such tasks are generally hard to solve within polynomial complexity, as even MAX-2-CUT is NP-hard. A breakthrough came with the work of Goemans and Williamson (GW) [GW95], who provided a randomized, polynomial-time approximation algorithm based on semidefinite programming (SDP) relaxations for the case of MAX-2-CUT, achieving an expected approximation ratio of 0.878. Following work by Frieze and Jerrum [FJ97] extended this approach to  $K > 2$ , providing a real-valued SDP relaxation and rounding scheme for

MAX-3-CUT. However, SDP-based algorithms often do not scale well, partially due to their inherent difficulty to run in parallel [MHA19]. Other methods for MAX-3-CUT include heuristic [PJ16, MH17, GJG18] and learning-based [AXSS19, BPL22, QXW+24, TKLG22, SBK22] algorithms. In this work, we study alternative algorithms that find exact solutions on a subclass of structured problems, recover theoretical approximation guarantees for perturbations of these structures, and allow for direct parallelization.

**Max-3-Cut as a complex ternary quadratic maximization problem.** In this work, we propose solutions to the following discrete quadratic maximization problem:

$$\text{OPT-Q}^* := \max_{\mathbf{z} \in \mathcal{A}_K^n} \mathbf{z}^\dagger \mathbf{Q}^* \mathbf{z}. \quad (2)$$

This problem generalizes the binary quadratic formulation representing MAX-CUT (1) to all  $K$ . Here,  $\mathbf{Q}^*$  is a Hermitian and positive-semidefinite (PSD) data matrix in  $\mathbb{C}^{n \times n}$  (e.g. a generalization of the Laplacian of a graph),  $\mathbf{z} \in \mathcal{A}_K^n$  is the discrete variable vector, and  $\mathcal{A}_K = \{ \exp(2k\pi i/K) : k \in \{0, 1, \dots, K-1\} \}$  makes up the  $K^{\text{th}}$  roots of unity, where  $i$  is the imaginary number. For  $K = 3$ , this complex ternary quadratic maximization problem represents MAX-3-CUT (see Appendix A for a derivation). However, as the  $K^{\text{th}}$  roots of unity for  $K > 3$  are not pairwise equidistant, this problem does not correspond to the MAX- $K$ -CUT problem. Nonetheless, this problem formulation appears in many applications for different  $K$  values [Kar72, BGJR88, GW95, DL94, Har96, SM00, MIMO17, GPI13, WJC13]. In this work, we present algorithms that solve (2) for general  $K$ , but focus our experiments on  $K = 3$  to specifically address the MAX-3-CUT problem.

**Toy example: approximating Max-2-Cut.** Our approach relies on low-rank approximations of the objective matrix  $\mathbf{Q}^*$  in (2). As a motivation, consider the MAX-2-CUT problem (2) with  $\mathcal{A}_2 = \{\pm 1\}$  and a real, rank-1 PSD matrix  $\mathbf{Q}^* = \lambda \mathbf{q} \mathbf{q}^\top$ . Here,  $\mathbf{q}$  denotes the real-valued eigenvector of  $\mathbf{Q}^*$  corresponding to the positive eigenvalue  $\lambda$ . Then, (2) can be written as:

$$\max_{\mathbf{z} \in \mathcal{A}_2^n} \mathbf{z}^\top \mathbf{Q}^* \mathbf{z} = \max_{\mathbf{z} \in \mathcal{A}_2^n} \lambda (\mathbf{z}^\top \mathbf{q})^2 = \lambda \cdot \max_{\mathbf{z} \in \mathcal{A}_2^n} (\mathbf{z}^\top \mathbf{q})^2.$$

Interestingly, this problem has a closed form maximizer [KL06]:  $\mathbf{z}^* = \text{sign}(\mathbf{q})$ . Finding this maximizer takes  $O(n^2)$  time, as it takes  $O(n^2)$  time to compute  $\mathbf{q}$ , and  $O(n)$  time to compute  $\mathbf{z}^*$  given  $\mathbf{q}$ . If one does not exploit the low-rank structure of  $\mathbf{Q}^*$ , an SDP-based solver [GW95] requires at best  $O(n^{3.5})$  complexity to find an approximate solution.

**Summary of contributions.** While this toy example illustrates how low-rank structure can be leveraged to efficiently and exactly solve the MAX-2-CUT problem, this approach does not readily extend to complex  $\mathbf{Q}^*$ ,  $K > 2$ , and for higher ranks of  $\mathbf{Q}^*$ . In this work, we address these challenges, studying the MAX-3-CUT problem under the assumption that  $\mathbf{Q}^*$  exhibits low-rank or approximately low-rank structure. Our key contributions are as follows:

1. **Exact algorithms for rank- $r$  matrices.** We provide algorithms for approximating the discrete quadratic maximization problem given in (2) that run in  $\mathcal{O}(rn^{2r+1})$  time for  $r \in \mathbb{N}$ . In particular, for general  $K$  and when the objective matrix has rank-1, our novel algorithm has complexity  $O(n^2)$ .
2. **Theoretical guarantees for approximately low-rank matrices.** Although our algorithms are exact only for low-rank objective matrices, we prove that they are also able to approximately recover the solution to (2) on a low-rank matrix after perturbation. Specifically, under a mild incoherence condition, assume the objective matrix has the structure  $\mathbf{Q} = \mathbf{Q}^* + \mathbf{H}$ , for some rank- $r$  matrix  $\mathbf{Q}^*$  and noise matrix  $\mathbf{H}$ . Then, by computing a low-rank approximation of  $\mathbf{Q}$  and running our rank- $r$  algorithm, we find an  $\left(1 - O\left(\frac{\|\mathbf{H}\|_2}{\delta}\right)\right)$ -approximation of (2) with objective  $\mathbf{Q}^*$ , where  $\delta$  relates to the spectral gap of  $\mathbf{Q}^*$ .
3. **Performance and scalability.** We provide a parallelized implementation of our algorithms applied to the MAX-3-CUT problem that combines a low-rank approximation of graph Laplacians with our exact low-rank algorithm. Experiments on synthetic graphs and established benchmarks demonstrate that this approach scales to graphs with tens of thousands of nodes. In particular, our algorithm

achieves up to a  $74\times$  speed-up compared to heuristic algorithms while preserving solution quality on structured graph instances.

**Notation.** Vectors and matrices are denoted in boldface (e.g.,  $\mathbf{v}$ ,  $\mathbf{Q}$ ), and scalars as plain letters (upper or lowercase). The  $i^{\text{th}}$  row and  $j^{\text{th}}$  column of a matrix  $\mathbf{A}$  are denoted  $\mathbf{A}_{i,:}$  and  $\mathbf{A}_{:,j}$ , respectively. The  $i^{\text{th}}$  entry of a vector  $\mathbf{z}$  is denoted  $z_i$ . Calligraphic uppercase letters are often used as sets (e.g.,  $\mathcal{A}$ ). For a positive integer  $n$ ,  $[n]$  denotes the set  $\{1, \dots, n\}$ .  $\hat{i}$  denotes the imaginary number, i.e.  $\hat{i} = \sqrt{-1}$ .  $|c| = \sqrt{\text{Re}(c)^2 + \text{Im}(c)^2}$  denotes the magnitude of the complex number  $c = \text{Re}(c) + \hat{i} \text{Im}(c) \in \mathbb{C}$ .  $\bar{c}$  and  $c^\dagger$  denote the complex conjugate of  $c \in \mathbb{C}$ , and  $\mathbf{c}^\dagger$  denotes the conjugate transpose of  $\mathbf{c} \in \mathbb{C}^n$ . We use  $\mathcal{N}_{\mathbb{C}}$  to denote the complex Gaussian distribution.

## 1.1 Related Work

**Low-rank approaches for Max-Cut.** “Low-rankness” for MAX-CUT has been traditionally connected to the Burer-Monteiro matrix factorization technique [AHO97, Bar95, Pat98]. This technique relies on an SDP relaxation enforcing low-rankness of the *solution to the SDP*. More precisely, for a Laplacian  $\mathbf{Q}$  and rank  $r$ , they formulate the SDP objective as  $\min_{\mathbf{U} \in \mathbb{R}^{n \times r}} \langle \mathbf{Q}, \mathbf{U}\mathbf{U}^\top \rangle$  s.t.  $\|\mathbf{U}_{i,:}\|_2 = 1 \forall i$ . Another line of work studies MAX-CUT algorithms on low-threshold rank graphs—graphs whose *adjacency matrices* have a small number of large eigenvalues [FK99, ABS11, BRS12, GT15]. Our work differs from these approaches in that we primarily study graphs with low-rank *Laplacians*, and we focus on MAX-3-CUT.

**Semidefinite programming relaxations.** Goemans and Williamson [GW95] provided a semi-definite programming (SDP) relaxation and a rounding scheme for MAX-2-CUT, achieving an approximation ratio of 0.878956, which was later shown to be optimal under the Unique Games Conjecture [KKMO07]. Frieze and Jerrum [FJ97] generalized [GW95] to the MAX- $K$ -CUT problem. Andersson et. al [AEH01] and De Klerk et. al. [dKPW04] similarly presented SDP relaxations and rounding schemes for the MAX-3-CUT problem. De Klerk et. al. [dKPW04] also gave an improved analysis of the algorithm of Frieze and Jerrum, proving an approximation ratio of 0.836008. Concurrent to De Klerk et. al., Goemans and Williamson [GW01] introduced a complex SDP relaxation and rounding scheme for MAX-3-CUT achieving the same ratio of 0.836008. Unlike prior works, their techniques do not easily extend to  $K > 3$  [GW01, New18]. As in the MAX-2-CUT case the approximation ratio of 0.836008 achieved by these SDP-based algorithms is optimal for MAX-3-CUT under the Unique Games conjecture [KKMO07].

**Spectral and heuristic approaches.** Heuristic-based approaches provide more efficient algorithms but often lack provable guarantees. Examples of heuristic approaches for MAX-3-CUT specifically include evolutionary algorithms [WH12, LZ13, PJ16, GGH24] and search algorithms [SSR12, BH13, SGS15, MH17, GJG18]. Singer [Sin11] presented a spectral method for the related problem of angular synchronization that also may be used for MAX-3-CUT. Due to the connections between MAX-3-CUT and graph 3-coloring, heuristic algorithms for coloring may also be used to solve MAX-3-CUT. These algorithms include degree of saturation [Br679], greedy independent set partitioning [LSS15], and simulated annealing [JAMS91].

**Learning-based approaches.** Recently, several machine learning-based approaches for MAX-CUT and MAX-3-CUT have been proposed. Some use reinforcement learning (RL) to learn heuristics or guide search algorithms [KDZ<sup>+</sup>17, BCFL20]. Others design train graph neural networks (GNNs) end-to-end to find optimal cuts by minimizing particular loss functions [YBV19, KL20, SBK22, QXW<sup>+</sup>24]. Many algorithms also combine these techniques, using GNNs as policy networks within RL frameworks [AXSS19, BPL22, TKLG22].

Despite the achievements by these learning-based methods, they remain largely black boxes that lack the theoretical guarantees of SDP-based algorithms and the interpretability of heuristic approaches. Additionally, they are highly data-driven, requiring large amounts of data and computational power to train from scratch. In contrast, *we provide a theoretically-motivated approach that operates out-of-the-box on any graph and runs on standard CPUs.*

## 2 Exact Rank-1 Algorithm

In the introduction, we gave a simple algorithm solving the binary quadratic maximization problem representing MAX-2-CUT (1) for a real, rank-1 matrix. In this section, we describe an algorithm which exactly solves the complex discrete quadratic maximization problem given in (2) for a complex rank-1 matrix  $\mathbf{Q}^*$  in polynomial time. This algorithm leverages the eigenvector of  $\mathbf{Q}^*$  to enumerate a set of  $n + 1$  candidate cuts and evaluates each cut within this set. We show that this set is guaranteed to contain the maximizer.

**Overview of Algorithm.** Let  $\mathbf{Q}^*$  be a rank-1, positive semi-definite matrix and consider the maximization problem given in (2) with objective matrix  $\mathbf{Q}^*$ . As  $\mathbf{Q}^*$  has rank-1, we can decompose it as  $\mathbf{Q}^* = \lambda \mathbf{q} \mathbf{q}^\dagger$ , where  $\mathbf{q} \in \mathbb{C}^n$  and  $\lambda > 0$ . Given this decomposition, we can reformulate (2) as the maximization of the magnitude of a complex inner product. Specifically, we have:

$$\mathbf{z}^\dagger \mathbf{Q}^* \mathbf{z} \propto |\mathbf{z}^\dagger \mathbf{q}|. \quad (3)$$

Note that any complex number (in this case,  $\mathbf{z}^\dagger \mathbf{q}$ ) can be rotated by a phase  $\varphi$  so that its magnitude equals its projection onto the real axis. We introduce an auxiliary phase variable  $\varphi \in (-\pi, \pi]$  and a rotation function  $c(\varphi) := e^{i\varphi}$  to represent this rotation. Employing (3) and this auxiliary variable, we can express the maximization problem (2) as:

$$\max_{\mathbf{z} \in \mathcal{A}_K^n} \mathbf{z}^\dagger \mathbf{Q}^* \mathbf{z} = \max_{\mathbf{z} \in \mathcal{A}_K^n} \max_{\varphi \in [-\pi, \pi)} \operatorname{Re}(\mathbf{z}^\dagger \mathbf{q} \cdot c(\varphi)) \quad (4)$$

$$= \max_{\varphi \in [-\pi, \pi)} \sum_{i=1}^n \max_{z_i \in \mathcal{A}_K} \operatorname{Re}(z_i^\dagger (q_i \cdot c(\varphi))). \quad (5)$$

A critical observation of this approach is that for a fixed  $\varphi$ , the choice of each  $z_i$  is independent. Specifically, the optimal  $z_i$  aligns as closely as possible with the direction of  $q_i \cdot c(\varphi)$ . As the auxiliary angle  $\varphi$  varies continuously over  $[-\pi, \pi)$ , the optimal choice for each  $z_i$  remains piecewise constant and changes only when the phase of  $q_i \cdot c(\varphi)$  crosses a decision boundary between two sectors in the complex plane. Because the roots of unity are symmetric with period  $2\pi/K$ , it is sufficient to restrict  $\varphi$  to an interval of width  $2\pi/K$ . Over such an interval, each element  $q_i$  crosses exactly one boundary point  $\varphi_i$ .

Algorithm 1 identifies and sorts these  $n + 1$  boundary points, partitioning the range of rotations into  $n + 1$  distinct cells. Within each cell, the assignment vector  $\mathbf{z}$  remains constant. Consequently, the algorithm only needs to enumerate and evaluate a candidate set of  $n + 1$  assignment vectors to guarantee that it finds the global optimum.

---

### Algorithm 1 Exact Solver of (2) for Rank-1 Matrix

---

- 1: **Input:** PSD matrix  $\mathbf{Q}^* \in \mathbb{C}^{n \times n}$ , singular vector  $\mathbf{q} \in \mathbb{C}^n$ , number of variables  $K$ .
  - 2: **Output:** Candidate solution  $\mathbf{z}^* \in \mathcal{A}_K^n$  for  $\max_{\mathbf{z}} \mathbf{z}^\dagger \mathbf{Q}^* \mathbf{z}$ .  $\mathbf{z}^*$  is optimal when  $\operatorname{rank}(\mathbf{Q}^*) = 1$ .
  - 3: **procedure** EXACT-RANK-1( $\mathbf{Q}^*$ ,  $K$ )
  - 4:    $\boldsymbol{\theta} \leftarrow \arctan\left(\frac{\operatorname{Im}(\mathbf{q})}{\operatorname{Re}(\mathbf{q})}\right) \in \mathbb{R}^n$  ▷ Compute the phase of each  $q_i$
  - 5:    $\varphi \leftarrow \frac{2\pi}{K} \left(\frac{1}{2} + \lfloor \frac{K\boldsymbol{\theta}}{2\pi} \rfloor - \frac{K\boldsymbol{\theta}}{2\pi}\right) \in \mathbb{R}^n$  ▷ Find the boundary points
  - 6:    $i_1, \dots, i_n \leftarrow \operatorname{ARGSORT}(\varphi)$
  - 7:    $\mathbf{k} \leftarrow \lfloor \frac{K\boldsymbol{\theta}}{2\pi} \rfloor \in \mathbb{R}^n$
  - 8:    $\mathcal{Z} \leftarrow \{\exp(\frac{2\pi i}{K} \cdot \mathbf{k})\}$  where  $|\mathcal{Z}| = 1$
  - 9:   **for**  $\ell \in [n]$  **do**
  - 10:      $\mathbf{k} \leftarrow \mathbf{k} + \mathbf{e}_{i_\ell} \pmod K$  ▷ Find candidate across the  $i_\ell^{\text{th}}$  boundary point
  - 11:      $\mathcal{Z} \leftarrow \mathcal{Z} \cup \{\exp(\frac{2\pi i}{K} \cdot \mathbf{k})\}$
  - 12:   **return**  $\arg \max_{\mathbf{z} \in \mathcal{Z}} \mathbf{z}^\dagger \mathbf{Q}^* \mathbf{z}$
- 

**Theoretical Guarantees.** We provide the following theorem:

**Theorem 1.** *Let  $\mathbf{Q}^* = \lambda \mathbf{q} \mathbf{q}^\dagger \in \mathbb{C}^n$  be a rank-1, positive semi-definite matrix. Algorithm 1 exactly solves the complex discrete quadratic maximization problem (2) with objective matrix  $\mathbf{Q}^*$  in  $\mathcal{O}(n^2)$  time.*

*Proof.*

**Time Complexity.** Given  $\mathbf{q}$ , calculating  $\theta$ ,  $\varphi$  and  $\mathbf{k}$  takes linear time  $\mathcal{O}(n)$ . Sorting the  $\varphi_i$ 's takes  $\mathcal{O}(n \log n)$  time. There are  $n+1$  such candidates. Algorithm 1 evaluates a quadratic form for each candidate  $\mathbf{z}$ . However, given access to  $\mathbf{q}$ , this quadratic form is  $|\mathbf{z}^\dagger \mathbf{q}|$  and may be evaluated in  $\mathcal{O}(n)$  time. This results in a total time complexity of  $\mathcal{O}(n^2)$ . We remark that these enumeration and evaluation steps are fully parallelizable—given  $P$  workers, each worker may find and evaluate  $\mathcal{O}(n/P)$  candidates, for an overall time complexity of  $\mathcal{O}(n^2/P)$ . Note that if  $\mathbf{q}$  is not given, its computation requires  $\mathcal{O}(n^2)$ , which does not increase the overall complexity.

**Correctness.** As established previously in this section, the discrete quadratic maximization problem (2) for a rank-1 matrix  $\mathbf{Q}^* = \lambda \mathbf{q} \mathbf{q}^\dagger$  is equivalent to:

$$\max_{\varphi \in [-\pi, \pi]} \sum_{i=1}^n \max_{z_i \in \mathcal{A}_K} \operatorname{Re} \left( z_i^\dagger q_i e^{i\varphi} \right). \quad (6)$$

As previously mentioned, because the roots of unity are periodic, we can restrict the range of  $\varphi$  to  $[-\pi/K, \pi/K]$ . For a fixed  $\varphi$  in this interval and  $i \in [n]$ , the inner maximization above is solved by choosing  $z_i$  to be the root of unity with the closest phase to the phase of  $q_i e^{i\varphi}$ . By the definition of  $\mathcal{A}_K$ , the phase of any root of unity  $z_i \in \mathcal{A}_K$  is  $\frac{2\pi k_i}{K}$  for some  $k_i \in \{0, \dots, K\}$ . Expressing  $q_i$  in polar coordinates as  $q_i = r_i e^{i\theta_i}$  for some  $r_i \in \mathbb{R}$  and  $\theta_i \in (0, 2\pi]$ , we find the phase of  $q_i e^{i\varphi}$  to be  $\theta_i + \varphi$ . The optimal  $z_i$  therefore corresponds to

$$k_i = \arg \min_{k \in \{0, \dots, K\}} \left| \frac{2\pi k}{K} - (\varphi + \theta_i) \right| = \left\lfloor \frac{K}{2\pi} (\varphi + \theta_i) + \frac{1}{2} \right\rfloor. \quad (7)$$

At the left endpoint of the interval  $[-\pi/K, \pi/K]$ , when  $\varphi = -\pi/K$ , the optimal choice of  $k_i$  is  $k_i^{(1)} = \lfloor \frac{K\theta_i}{2\pi} \rfloor$ . When the phase  $\theta_i + \varphi$  crosses the midpoint between the phases involving  $k_i$  and  $k'_i = (k_i + 1) \bmod K$ , the solution to this inner maximization transitions to the root of unity corresponding to  $k'_i$ . For a given  $i$ , this midpoint is

$$\varphi_i = \frac{1}{2} \left( \frac{2\pi k_i}{K} + \frac{2\pi k'_i}{K} \right) - \theta_i = \frac{2\pi}{K} \left( \frac{1}{2} + \left\lfloor \frac{K\theta_i}{2\pi} \right\rfloor - \frac{K\theta_i}{2\pi} \right). \quad (8)$$

The phases  $\{\varphi_i\}_{i=1}^n$  are boundary points which partition the interval  $[-\pi/K, \pi/K]$  into  $n+1$  cells. Within each cell, the solution,  $\mathbf{z}$ , to the inner maximization of (6) remains constant. The solution to the entire maximization problem is guaranteed to be contained within one such cell. Algorithm 1 evaluates the solution, or candidate vector, corresponding to each cell, and returns the candidate which maximizes  $\mathbf{z}^\dagger \mathbf{Q}^* \mathbf{z}$ .  $\square$

### 3 Exact Rank- $r$ Algorithm

Generalizing the rank-1 approach, our rank- $r$  algorithm reformulates the discrete quadratic problem (2) as a double maximization over an auxiliary angular parameter  $\varphi \in \mathcal{H}_r$ . The algorithm partitions the high-dimensional search space into cells within which the candidate vector remains constant. By identifying the vertices of this partition, we construct a polynomial-size set of candidate vectors guaranteed to contain the global optimizer. This approach is adapted from [KK14] to handle general alphabet size  $K$ .

**Overview of Algorithm.** Let  $\mathbf{Q}_r$  be a rank- $r$ , positive semi-definite (PSD) matrix. Again, consider the maximization problem (2) with objective matrix  $\mathbf{Q}_r$ . Because  $\mathbf{Q}_r$  is PSD and has rank  $r$ , we can decompose it as  $\mathbf{Q}_r = \mathbf{V} \mathbf{V}^\dagger$  for some matrix  $\mathbf{V} \in \mathbb{C}^{n \times r}$ . We can use this decomposition to reformulate (2) as the maximization of the norm of a complex vector-matrix product:

$$\max_{\mathbf{z} \in \mathcal{A}_K^n} \mathbf{z}^\dagger \mathbf{Q}_r \mathbf{z} \propto \max_{\mathbf{z} \in \mathcal{A}_K^n} \|\mathbf{z}^\dagger \mathbf{V}\|_2. \quad (9)$$

As in the rank-1 case, the norm of this vector-matrix product can be recovered by selecting the maximum direction that aligns it with the real axis. To represent this alignment, we introduce an auxiliary unit vector

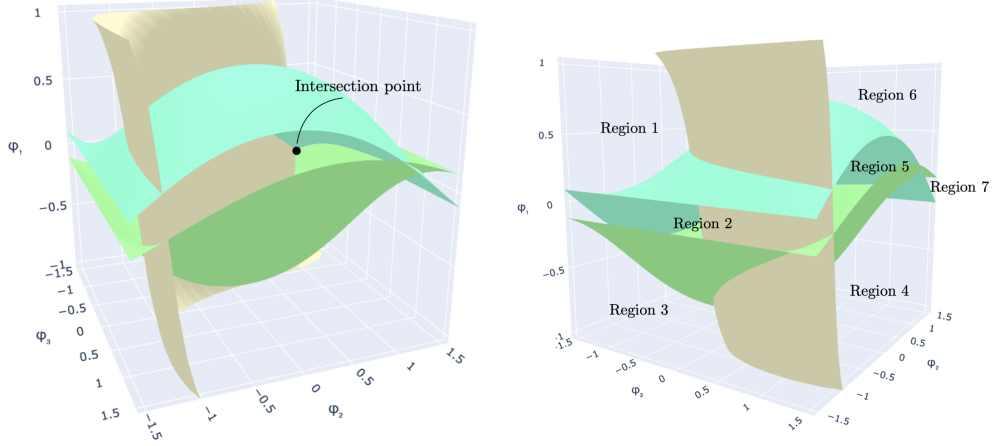


Figure 1: A toy example of the partition of the hypercube  $\mathcal{H}_r$  formed by  $2r - 1$  hypersurfaces, with  $r = 2$ . Each region, or cell, of the partition corresponds to a different candidate cut.

$\mathbf{c}(\boldsymbol{\varphi}) \in \mathbb{C}^r$ , parametrized by a vector of angular coordinates  $\boldsymbol{\varphi} \in \mathcal{H}_r$ . The range of  $\boldsymbol{\varphi}$  is a hypercube  $\mathcal{H}_r$  defined as:

$$\mathcal{H}_r := \left(-\frac{\pi}{2}, \frac{\pi}{2}\right]^{2(r-1)} \times \left(-\frac{\pi}{K}, \frac{\pi}{K}\right]. \quad (10)$$

Using these auxiliary variables, we expand (9) as:

$$\max_{\mathbf{z} \in \mathcal{A}_K^n} \|\mathbf{z}^\dagger \mathbf{V}\| = \max_{\mathbf{z} \in \mathcal{A}_K^n} \max_{\boldsymbol{\varphi} \in \mathcal{H}_r} \operatorname{Re}(\mathbf{z}^\dagger \mathbf{V} \mathbf{c}(\boldsymbol{\varphi})) = \max_{\boldsymbol{\varphi} \in \mathcal{H}_r} \sum_{i=1}^n \max_{z_i \in \mathcal{A}_K} \operatorname{Re}\{z_i^\dagger \mathbf{V}_{i,:} \mathbf{c}(\boldsymbol{\varphi})\}. \quad (11)$$

Similarly to the rank-1 formulation, we observe that for any fixed  $\boldsymbol{\varphi}$ , the optimal choice of each  $z_i$  in (11) is independent. For a given  $i \in [n]$ , the optimal  $z_i \in \mathcal{A}_K$  is that which is closest in phase to  $\mathbf{V}_{i,:} \mathbf{c}(\boldsymbol{\varphi})$ . A change in the optimal  $z_i$  occurs only when the vector  $\mathbf{V}_{i,:} \mathbf{c}(\boldsymbol{\varphi})$  crosses a particular decision boundary, represented by a ray in the complex plane.

**Decision Boundary Structure.** The number of decision boundaries per coordinate depends critically on the alphabet size  $K$ . For each  $i \in [n]$ , the decision boundaries correspond to the  $K$  rays that bisect adjacent symbols in  $\mathcal{A}_K$ , located at angles  $\vartheta_m = \frac{\pi(2m+1)}{K}$  for  $m \in \{0, 1, \dots, K-1\}$ . However, not all of these boundaries are geometrically distinct.

For alphabet size  $K \geq 2$ , the number of distinct decision boundaries per coordinate is:

$$B_K = \begin{cases} K/2 & \text{if } K \text{ is even,} \\ K & \text{if } K \text{ is odd.} \end{cases} \quad (12)$$

This distinction arises from antipodal symmetry: for even  $K$ , the element  $-1 \in \mathcal{A}_K$ , causing boundary rays at angles  $\vartheta_m$  and  $\vartheta_m + \pi$  to define the same hyperplane in the auxiliary parameter space. For odd  $K$  (including primary case  $K = 3$ ), no two boundary angles differ by exactly  $\pi$ ; all  $K$  boundaries are distinct. For Max-3-Cut, we have  $B_3 = 3$  decision boundaries per coordinate, compared to  $B_2 = 1$  for the binary case.

**Augmented Matrix Construction.** By introducing an augmented real matrix  $\tilde{\mathbf{V}} \in \mathbb{R}^{nB_K \times 2r}$  and auxiliary vector  $\tilde{\mathbf{c}}(\boldsymbol{\varphi}) \in \mathbb{R}^{2r}$ , we express all decision boundaries as a system of real linear equations. The augmented

matrix is constructed by stacking  $B_K$  rotated copies of the factor matrix:

$$\tilde{\mathbf{V}} = \begin{bmatrix} \Re\{\rho_0 \mathbf{V}\} & \Im\{\rho_0 \mathbf{V}\} \\ \Re\{\rho_1 \mathbf{V}\} & \Im\{\rho_1 \mathbf{V}\} \\ \vdots & \vdots \\ \Re\{\rho_{B_K-1} \mathbf{V}\} & \Im\{\rho_{B_K-1} \mathbf{V}\} \end{bmatrix}, \quad (13)$$

where  $\rho_m = e^{-i\pi(2m+1)/K}$ .

For all  $j \in [nB_K]$ , the solution to  $\tilde{\mathbf{V}}_{j,:} \tilde{\mathbf{c}}(\boldsymbol{\varphi}) = 0$  yields a  $(2r - 2)$ -dimensional manifold (hypersurface) within the hypercube  $\mathcal{H}_r$ . The set of all  $nB_K$  hypersurfaces partitions the hypercube into cells, with each cell corresponding to a unique candidate vector in  $\mathcal{A}_K^n$ , just as each interval in the rank-1 case corresponds to a candidate vector. Figure 1 provides an illustration of this partition.

A key structural property simplifies the enumeration: all  $B_K$  hypersurfaces originating from the same coordinate  $i$  share a common  $(2r - 3)$ -dimensional intersection, namely the locus where  $\mathbf{V}_{i,:} \mathbf{c}(\boldsymbol{\varphi}) = 0$ . This means that selecting more than two hypersurfaces from the same coordinate group leads to rank deficiency in the defining system. We exploit this property to efficiently enumerate only the valid vertex configurations; see Appendix C for the complete analysis.

**Vertex Enumeration.** To systematically identify all candidates, our algorithm examines the vertices of the cell partition. In the  $(2r - 1)$ -dimensional hypercube  $\mathcal{H}_r$ , each vertex is defined by the intersection of  $2r - 1$  hypersurfaces. Therefore, we identify these vertices by solving, for all valid combinations  $I \subset [nB_K]$  of size  $2r - 1$ , the local system given by  $\tilde{\mathbf{V}}_{I,:} \tilde{\mathbf{c}}(\boldsymbol{\varphi}) = \mathbf{0}$ . An index set  $I$  is *valid* if it contains at most two indices from any single coordinate group—a necessary condition for the submatrix  $\tilde{\mathbf{V}}_{I,:}$  to have full rank.

Each solution  $\boldsymbol{\varphi}_I$  maps to a candidate vector  $\mathbf{z}_I$  by the following decision rule:

$$\mathbf{z}_I = \mathbf{d}(\mathbf{V}; \boldsymbol{\varphi}_I) = \exp\left(\frac{2\pi i}{K} k_i\right), \quad (14)$$

$$\text{where } k_i = \arg \min_{k \in \{0, 1, \dots, K-1\}} \left| \frac{2\pi k}{K} - \arg(\mathbf{V}_{i,:} \mathbf{c}(\boldsymbol{\varphi})) \right|_{\text{mod } 2\pi}. \quad (15)$$

In addition to the cell vertices, the algorithm must identify candidates that land on the boundaries of the hypercube. These boundary cases occur when one component of  $\boldsymbol{\varphi}$  is fixed, and therefore correspond to lower-rank subproblems. They are solved by recursive calls to the rank- $(r - 1)$  algorithm [KK11]. By evaluating the candidate vectors found by the valid combinations and the rank- $(r - 1)$  recursion, we construct a polynomial-size feasible candidate set that is guaranteed to contain the global optimizer.

**Remark 2** (Parallelizability). *The candidate enumeration and evaluation steps of Algorithm 2 are embarrassingly parallel, as each index set  $\mathcal{I}$  can be processed independently. With  $P$  processors, the parallel complexity is  $\mathcal{O}(rn^{2r+1}/P)$ .*

**Theoretical Guarantees.** We provide the following theorem. The proof is given in Appendix B.

**Theorem 3.** *Let  $\mathbf{Q}_r \in \mathbb{C}^{n \times n}$  be a rank- $r$ , positive semi-definite matrix. Algorithm 2 solves the discrete quadratic maximization problem (2) with objective matrix  $\mathbf{Q}_r$  in  $\mathcal{O}(rn^{2r+1})$  time.*

## 4 Approximate Algorithms for Perturbed Low-Rank Graphs

Algorithms 1 and 2 are guaranteed to find the exact maximizer of (2) for low-rank  $\mathbf{Q}^*$ . However, the assumption that  $\mathbf{Q}^*$  is low-rank is restrictive in practice; when  $\mathbf{Q}^*$  represents the Laplacian of a graph (as in the motivating example of MAX-3-CUT), its rank is the difference between the number of nodes in the graph and the number of connected components, the latter of which is often constant. In this section, we prove that our algorithm can approximately recover the solution to (2) with rank- $r$  objective matrix  $\mathbf{Q}^*$ , even when run on a perturbation of this matrix.

---

**Algorithm 2** Exact Solver of (2) for Rank- $r$  Matrix [KK11, KK14]

---

```

1: input PSD matrix  $\mathbf{Q} \in \mathbb{C}^{n \times n}$ , matrix of ordered singular vectors  $\mathbf{V}$ , rank  $r$ , alphabet size  $K$ .
2: output Candidate  $\mathbf{z}^* \in \mathcal{A}_K^n$  for  $\max_{\mathbf{z}} \mathbf{z}^\dagger \mathbf{Q} \mathbf{z}$ .  $\mathbf{z}^*$  is optimal when  $\text{rank}(\mathbf{Q}) = r$ .
3: procedure EXACT-LOW-RANK( $\mathbf{Q}, \mathbf{V}, r, K$ )
4:   Construct augmented matrix  $\tilde{\mathbf{V}} \in \mathbb{R}^{nB_K \times 2r}$  from  $\mathbf{V}$ . ▷ See (13).
5:    $\text{opt} \leftarrow -\infty$ ;  $\mathbf{z}^* \leftarrow \mathbf{0}$ 
6:    $\mathcal{I} \leftarrow \{I \subset [nB_K] : |I| = 2r - 1, \text{ at most 2 indices per coordinate group}\}$ 
7:   for  $I \in \mathcal{I}$  do ▷ Generate and evaluate candidates.
8:     if  $\text{rank}(\tilde{\mathbf{V}}_{I,:}) = 2r - 1$  then
9:       Solve  $\tilde{\mathbf{V}}_{I,:} \tilde{\mathbf{c}} = \mathbf{0}$  for  $\tilde{\mathbf{c}} \in \mathbb{R}^{2r} \setminus \{\mathbf{0}\}$ 
10:       $\mathbf{c} \leftarrow \tilde{\mathbf{c}}_{1:r} + i\tilde{\mathbf{c}}_{r+1:2r}$ 
11:       $\mathbf{z} \leftarrow \text{DECISIONRULE}(\mathbf{V}, \mathbf{c})$  ▷ See (14).
12:      if  $\text{Re}(\mathbf{z}^\dagger \mathbf{Q} \mathbf{z}) > \text{opt}$  then
13:         $\text{opt} \leftarrow \text{Re}(\mathbf{z}^\dagger \mathbf{Q} \mathbf{z})$ ;  $\mathbf{z}^* \leftarrow \mathbf{z}$ 
14:   if  $r > 1$  then ▷ Recursively call lower-rank algorithm.
15:      $\mathbf{z}_{r-1} \leftarrow \text{EXACT-LOW-RANK}(\mathbf{Q}, \mathbf{V}_{::,r-1}, r-1, K)$ 
16:     if  $\text{Re}(\mathbf{z}_{r-1}^\dagger \mathbf{Q} \mathbf{z}_{r-1}) > \text{opt}$  then
17:        $\text{opt} \leftarrow \text{Re}(\mathbf{z}_{r-1}^\dagger \mathbf{Q} \mathbf{z}_{r-1})$ ;  $\mathbf{z}^* \leftarrow \mathbf{z}_{r-1}$ 
18:   return  $\mathbf{z}^*$ .

```

---

Specifically, we consider the solutions recovered by Algorithm 3. Algorithm 3 computes the approximate solution to the discrete quadratic optimization problem (2) with any objective matrix  $\mathbf{Q}$  by first constructing a low-rank approximation of the Laplacian of  $\mathbf{Q}$ , then running our rank- $r$  algorithm to find an exact solution to (2) with this low-rank matrix as the objective. When  $K = 3$  and the input matrix  $\mathbf{Q}$  represents the Laplacian of a graph  $\mathcal{G}$ , this algorithm provides an approximate solution to the MAX-3-CUT of  $\mathcal{G}$ .

---

**Algorithm 3** Approximate Solver of (2) via Low-Rank Approximations

---

```

1: procedure APPROXIMATE-LOW-RANK( $\mathbf{Q}, r, K$ )
2:    $\Sigma_r \leftarrow$  top- $r$  singular values of  $\mathbf{Q}$ 
3:    $\mathbf{V}_r \leftarrow$  top- $r$  left singular vectors of  $\mathbf{Q}$ 
4:    $\mathbf{Q}_r \leftarrow \mathbf{V}_r \Sigma_r \mathbf{V}_r^\dagger$ 
5:   return EXACT-LOW-RANK( $\mathbf{Q}_r, \mathbf{V}_r, r, K$ )

```

---

**Low-rank Structure with Perturbation.** To provide a theoretical justification of our approach, we study the case when the input matrix to Algorithm 3,  $\mathbf{Q}$ , has an underlying low-rank structure, possibly with some perturbation. Specifically, assume

$$\mathbf{Q} = \mathbf{Q}^* + \mathbf{H}, \quad (16)$$

where  $\mathbf{Q}^* \succeq 0$  is a Hermitian, rank- $r^*$  matrix of interest such that  $\mathbf{Q}^* = \sum_{i=1}^{r^*} \lambda_i^* \mathbf{u}_i^* \mathbf{u}_i^{*\dagger}$  with  $r^* \ll n$ , and  $\mathbf{H} \in \mathbb{C}^{n \times n}$  is a matrix representing a perturbation. Note here that  $\mathbf{Q}$  may not be Hermitian or PSD.

Assume that we run Algorithm 3 on  $\mathbf{Q}$  with input rank  $r$ . Algorithm 3 finds a rank- $r$  approximation,  $\mathbf{Q}_r$ , of  $\mathbf{Q}$ , and solves  $\max_{\mathbf{z}} \mathbf{z}^\dagger \mathbf{Q}_r \mathbf{z}$ . Define the relevant complex quadratic optimization problems and their maximizers as:

$$\begin{aligned} \mathbf{z}^* \text{ attains } \text{OPT-}\mathbf{Q}^* &:= \max_{\mathbf{z} \in \mathcal{A}_K^n} \mathbf{z}^\dagger \mathbf{Q}^* \mathbf{z} \\ \mathbf{z}_r \text{ attains } \text{OPT-}\mathbf{Q}_r &:= \max_{\mathbf{z} \in \mathcal{A}_K^n} \mathbf{z}^\dagger \mathbf{Q}_r \mathbf{z} \end{aligned} \quad (17)$$

We aim to investigate the quality of the approximate solution  $\mathbf{z}_r$  in terms of its quadratic form defined over the signal matrix  $\mathbf{Q}^*$ , namely  $\mathbf{z}_r^\dagger \mathbf{Q}^* \mathbf{z}_r$ , by using  $\text{OPT-}\mathbf{Q}^*$  as a reference. Our theory applies to a general  $K \geq 2$ .

**Additive Bounds.** Theorem 4 describes the additive error of the approximation of  $\text{OPT-}\mathbf{Q}^*$  obtained by

Algorithm 3. The proof is provided in Appendix D.2.

**Theorem 4.** Let  $\mathbf{z}_r, \text{OPT}-\mathbf{Q}^*$  be defined in (17). Let  $\lambda_j^*$  be the  $j$ th eigenvalue of  $\mathbf{Q}^*$  with  $\lambda_j^* = 0$  if  $j > r$ , and define the eigengap of  $\mathbf{Q}$  as  $\delta^* = \min \{ \min_{j \in [r-1]} |\lambda_j^* - \lambda_{j+1}^*|, \lambda_r^* \}$ . If  $r \leq r^*$  and  $\|\mathbf{H}\|_2 \leq \frac{\delta^*}{2}$ , then we have that:

$$|\text{OPT}-\mathbf{Q}^* - \mathbf{z}_r^\dagger \mathbf{Q}^* \mathbf{z}_r| \leq O \left( n \left( \lambda_{r+1}^* + \frac{\lambda_1^*}{\delta^*} \|\mathbf{H}\|_2 \right) \right). \quad (18)$$

Theorem 4 upper bounds the gap between the quadratic form  $\mathbf{z}_r^\dagger \mathbf{Q}^* \mathbf{z}_r$  and  $\text{OPT}-\mathbf{Q}^*$ . The scaling factor of  $n$  in the right-hand side of (18) is due to the fact that both  $\text{OPT}-\mathbf{Q}^*$  and  $\mathbf{z}_r^\dagger \mathbf{Q}^* \mathbf{z}_r$  are quadratic in  $\mathbf{z}^*$  and  $\mathbf{z}_r$ , which has  $\ell_2$ -norm  $\sqrt{n}$  by construction. In particular, the right-hand side of the upper bound in (18) consists of two components. The first component,  $n\lambda_{r+1}^*$ , scales with the eigenvalue  $\lambda_{r+1}^*$ , and can be regarded as the price one pays when using a rank less than that of  $\mathbf{Q}^*$ , i.e.  $r \leq r^*$ . The second term depends on the noise scale  $\|\mathbf{H}\|_2$ , showing the influence of the perturbation on the quality of the solution.

**Multiplicative Bounds.** To compare Algorithm 3’s guarantees to those of existing methods, we develop a bound on its multiplicative approximation ratio. By assuming the incoherence condition [CCF18], Theorem 5 shows that the ratio of the solution induced by the low-rank approximation and the true solution of the underlying problem is bounded from 1 by a quantity depending on both the condition number of the rank truncation and the noise-scale over the eigengap. The proof is provided in Appendix D.5.

**Theorem 5.** Let  $\mathbf{Q}^*$  be a rank- $r$  Hermitian matrix. Let  $\mathbf{H} \in \mathbb{C}^{n \times n}$ . Assume we observe  $\mathbf{Q} = \mathbf{Q}^* + \mathbf{H}$ . Let  $\mathbf{z}_r$  be the output of (17) with  $K \geq 3$ . Recall that  $\mathbf{u}_i^*$  is the  $i$ th eigenvector of  $\mathbf{Q}^*$ . If  $\mathbf{Q}^*$  satisfies the incoherence condition  $\|\mathbf{u}_1^*\|_\infty \leq \frac{\mu}{\sqrt{n}}$ , where  $\mu$  is some absolute constant, then

$$\frac{\mathbf{z}_r^\dagger \mathbf{Q}^* \mathbf{z}_r}{\text{OPT}-\mathbf{Q}^*} \geq 1 - O \left( \frac{\lambda_{r+1}^*}{\lambda_1^*} + \frac{\|\mathbf{H}\|_2}{\delta^*} \right). \quad (19)$$

## 5 Experiments

We evaluate the practical performance of Algorithm 3 for MAX-3-CUT, comparing against standard heuristic methods on synthetic graph families and established benchmark instances. Extended results are available in Appendix E.

### 5.1 Experimental Setup.

*Graph Families.* We conduct experiments on three families of graphs: (i)  $\mathcal{G}(n, p)$  (Erdős-Rényi) random graphs with  $n = 20, 50$ , and  $100$ , and  $p = 0.1, 0.25, 0.5, 0.75$  and  $0.9$ ; (ii) Random  $d$ -regular graphs on  $n = 20, 50$  and  $100$  nodes, with  $d = 3, 4$  and  $5$ ; (iii) All GSet benchmark instances [Ye03]. GSet is a benchmark commonly used to evaluate MAX-K-CUT algorithms that consists of 71 graphs ranging in size from 800 to 20,000 nodes. Each GSet graph falls into one of the following categories [DH11]:

1. Erdos-Renyi graphs with edge probability at most 0.03,
2. 2-D toroidal, 4-regular graphs,
3. random graphs with skewed degree distributions.

These graphs either have binary (0 or 1) edge weights or have edge weights in  $\{-1, 0, +1\}$ .

*Baseline Algorithms.* We compare our algorithms to the following baselines: (i) FRIEZE-JERRUM [FJ97]: an SDP relaxation and rounding scheme; (ii) GREEDY [GJG18]: a greedy algorithm that iteratively identifies and locks the single-best node assignment; (iii) GENETIC [PJ16]: a genetic algorithm that maintains a set of candidate cuts and iteratively selects the best of this set, mixes pairs of cuts, and randomly perturbs the worst. On the GSet benchmark, we also compare to a random baseline, RANDOM. To ensure a fair comparison to RANK-1, RANDOM generates  $n + 1$  random cuts and selects the best one, matching the number of candidate solutions enumerated by our algorithm.

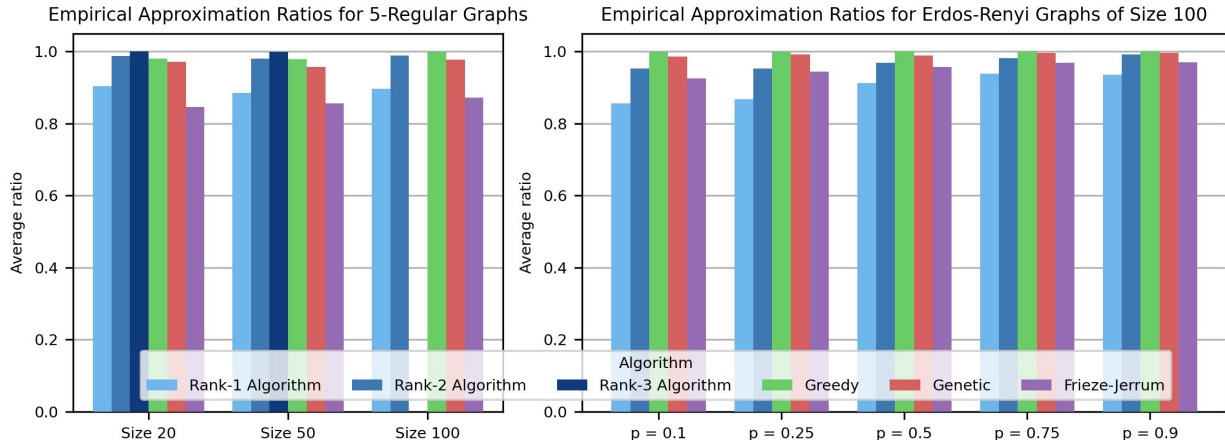


Figure 2: Empirical approximation ratios of the studied algorithms on 5-regular graphs of varying sizes (left) and on Erdős-Rényi graphs with  $n = 100$  nodes and varying edge probabilities (right).

*Implementation Details.* All experiments were conducted on HPE ProLiant DL360 Gen11 compute nodes (Sapphire Rapids) equipped with Intel Xeon Platinum 8468 CPUs (96 cores at 2.10 GHz). We generate 20 instances for each size and parameter of the small random graphs using the NetworkX library [HSS08] with fixed random seeds. We use the implementation of [QXW<sup>+</sup>24] for the GREEDY and GENETIC algorithms. We institute a 30-minute timeout limit for all experiments.

*Evaluation Metrics.* To measure the quality of the MAX-3-CUT approximations found by each algorithm on random graphs, we calculate the ratio of its score to the best score found by any algorithm. We report the average ratio across all random seeds.

*Parallel Implementation.* We develop a parallel implementation of Algorithm 2 using the Ray framework [MNW<sup>+</sup>18]. Observe that the dominant cost in Algorithm 2 is the cost to enumerate a polynomially-sized set of candidates  $z_I$  and compute a quadratic form for each candidate. In our implementation, we parallelize these enumeration and evaluation steps by mapping disjoint batches of candidates to Ray tasks. We choose the number of candidates in each batch heuristically based on the total number of candidates (which depends on  $n$  and  $r$ ). To make this enumeration tractable in memory, we generate batches of candidates as a stream, so that the implementation never materializes the full set of  $\binom{n}{2r-1}$  combinations. We also leverage Ray’s distributed object store to broadcast large read-only inputs (including  $\tilde{\mathbf{V}}$ ,  $\mathbf{V}$ , and  $\mathbf{Q}$ ) only once.

## 5.2 Small-Scale Experiments

On Erdős-Rényi and regular graphs of size 20 and 50, we compare the cuts found by our RANK-1, RANK-2, and RANK-3 algorithms to those of FRIEZE-JERRUM, GREEDY and GENETIC. For graphs of size 100, we compare only our RANK-1 and RANK-2 algorithms to the same baselines, omitting the RANK-3 algorithm due to its high computational costs as  $n$  increases. In Figure 2 (left), we plot the average empirical approximation ratios of these algorithms on random 5-regular graphs of sizes 20, 50 and 100. In Figure 2 (right), we plot the average empirical approximation ratios of these algorithms on Erdős-Rényi graphs with  $n = 100$  nodes and edge probabilities  $p \in \{0.1, 0.25, 0.5, 0.75, 0.9\}$ . Additional results on small graphs ( $n \leq 100$ ) are included in Appendix E.

Our results in Figure 2 (left) demonstrate that our low-rank approximations consistently compete with the heuristic and SDP-based baselines. On 5-regular graphs with 20 and 50 nodes, our RANK-3 algorithm achieves the highest average empirical approximation ratio, while our RANK-2 algorithm effectively matches the solution quality of GREEDY, the best-performing baseline, and our RANK-1 algorithm outperforms the FRIEZE-JERRUM algorithm. On graphs with 100 nodes, we observe that our RANK-2 algorithm remains competitive with GREEDY and maintains an advantage over FRIEZE-JERRUM.

Table 1: Comparison of our RANK-1 algorithm against RANDOM, GREEDY, GENETIC and MOH on select GSet instances. Reported values are scores of MAX-3-CUT approximations with runtimes in seconds in parentheses. Values for MOH are taken from [MH17] and runtimes are not compared due to likely hardware differences. Structural information about each graph is drawn from [DH11].

Case	$n$	Type	$\{0, 1\}$	GREEDY	MOH	RANK-1
<b>G1</b>	800	Erdos-Renyi	Yes	14859 (16.3s)	15165	13331 (1.09s)
<b>G7</b>	800	Erdos-Renyi	No	2082 (11.4s)	2409	992 (0.64s)
<b>G11</b>	800	Toroidal	No	619 (11.5s)	669	426 (0.51s)
<b>G14</b>	800	Skew	Yes	3914 (11.5s)	4012	3217 (0.56s)
<b>G19</b>	800	Skew	No	952 (11.4s)	1081	483 (0.49s)
<b>G48</b>	3,000	Toroidal	Yes	5998 (300s)	6000	6000 (5.2s)
<b>G49</b>	3,000	Toroidal	Yes	5996 (394s)	6000	6000 (5.3s)
<b>G50</b>	3,000	Toroidal	Yes	5998 (399s)	6000	5934 (5.9s)
<b>G67</b>	10,000	Toroidal	No	timeout	8086	3117 (76s)
<b>G81</b>	20,000	Toroidal	No	timeout	16321	4122 (352s)

In Figure 2 (right), we find that the solution quality of our RANK-2 algorithm increases with the density of Erdős-Rényi graphs with  $n = 100$  nodes. As the edge probability increases, the performance of our RANK-2 algorithm converges towards that of GREEDY. We also observe that our RANK-2 algorithm outperforms FRIEZE-JERRUM across all sparsity levels. However, especially in the sparse case, we find that our RANK-1 algorithm fails to match the solution quality of the baselines, suggesting that a rank-1 approximation of the Laplacian may be insufficient to capture the cut structure of sparse, random graphs.

### 5.3 Large-Scale Experiments

We perform large-scale experiments to compare the runtime and cuts found by our RANK-1 algorithm to the baselines on all GSet instances. In Table 1, we compare the cuts and wall-clock times of our algorithm to GREEDY on various GSet graphs. We also include the scores of cuts found by MOH, a heuristic algorithm achieving many of the best known results for MAX-3-CUT on GSet [MH17].

Our Rank-1 algorithm demonstrates a clear advantage over GREEDY in terms of runtime and scalability. On the smallest GSet instances (with  $n = 800$  nodes), the RANK-1 algorithm is about  $15 - 23\times$  faster. As the problem size increases, this gap widens. On binary toroidal graphs (G48, G49, and G50), the RANK-1 algorithm runs in under 6 seconds, whereas GREEDY requires over 5 minutes, demonstrating a speedup of roughly  $57 - 74\times$ . On the largest GSet instances, GREEDY fails to converge within a 30 minute cutoff, while the RANK-1 algorithm finishes in 76 and 352 seconds on G67 and G81, respectively.

In addition to its scalability, we observe that our algorithm performs exceptionally well on unweighted toroidal graphs, the most structured instances of GSet. On G48 and G49, the RANK-1 algorithm achieves a theoretically optimal cut value of 6,000, matching the solution quality MOH and slightly outperforming GREEDY. Similarly, on G50, our algorithm finds a near-optimal cut value of 5934. These results suggest that for highly-structured graphs, a rank-1 approximation is sufficient to capture the global structure. However, on less structured instances, we observe a trade-off between efficiency and solution quality.

### 5.4 Very Large Graphs.

To push the limits of our RANK-1 algorithm, we generate two random, 3-regular graph, one with 100,000 nodes and another with 50,000 nodes, and test our RANK-1 algorithm against RANDOM with 800 workers and no timeout limit. On the 100,000 node graph, our algorithm finishes in 61757 seconds (roughly 17 hours and 9 minutes) and finds a cut value of 137796, while the random algorithm requires 8269 seconds (2 hours and 18 minutes) and finds a cut value of 100781. On the 50,000 node graph we observe the same pattern: RANK-1 finished in 6597 seconds (roughly 1 hour and 49 minutes) and finds a cut value of 68951, while RANDOM finishes in 1345 seconds (roughly 22 minutes) and finds a cut value of 50517. We note that most of

the running time (about 14.5 hours for 100,000 node graph and 1.4 hours for the 50,000 node graph) of the RANK-1 algorithm is spent finding the principal eigenvector of the graph Laplacian. In applications where this is given or can be easily derived, our algorithm would run only slightly slower than RANDOM, while finding significantly better cuts.

## 6 Conclusion

We propose a family of algorithms for solving MAX-3-CUT and related quadratic maximization problems in both real and complex domains. These algorithms use low-rank approximations of the objective matrices to generate polynomially-sized sets of candidate cuts. On the theoretical side, we analyze the error introduced by our low-rank approximation scheme for matrices with perturbed low-rank structure. Empirically, we show that our RANK-2 and RANK-3 algorithms demonstrate performance comparable to state-of-the-art heuristic approaches on a suite of small synthetically-generated graphs. We demonstrate that our RANK-1 algorithm matches the state-of-the-art in solution quality on large, highly-structured graphs, and finds high-quality solutions for many less-structured graphs in a fraction of the time of heuristic algorithms. Finally, we highlight the parallelizability of our approach: our algorithms naturally lend themselves to distributed computing environments, enabling efficient solvers for MAX-3-CUT.

## 7 Acknowledgments

R.S. acknowledges partial support from the Ken Kennedy Institute Research Cluster Fund, the Ken Kennedy Institute Computational Science and Engineering Recruiting Fellowship, funded by the Energy HPC Conference and the Rice University Department of Computer Science, and the Ken Kennedy Institute 2025/26 Andrew Ladd Memorial Excellence in Computer Science Graduate Fellowship.

## References

- [ABS11] Sanjeev Arora, Boaz Barak, and David Steurer. Subexponential algorithms for unique games and related problems. *Journal of the ACM*, 58(5), 2011.
- [AEH01] Gunnar Andersson, Lars Engebretsen, and Johan Håstad. A new way of using semidefinite programming with applications to linear equations mod  $p$ . *Journal of Algorithms*, 39(2):162–204, 2001.
- [AHO97] F. Alizadeh, J. Haeberly, and M. Overton. Complementarity and nondegeneracy in semidefinite programming. *Mathematical programming*, 77(1):111–128, 1997.
- [AXSS19] Kenshin Abe, Zijian Xu, Issei Sato, and Masashi Sugiyama. Solving np-hard problems on graphs with extended alphago zero. *arXiv preprint arXiv:1905.11623*, 2019.
- [BAL19] Eric Benhamou, Jamal Atif, and Rida Laraki. Operator norm upper bound for sub-gaussian tailed random matrices, 2019.
- [Bar95] A. Barvinok. Problems of distance geometry and convex properties of quadratic maps. *Discrete & Computational Geometry*, 13(2):189–202, 1995.
- [BCFL20] Thomas Barrett, William Clements, Jakob Foerster, and Alex Lvovsky. Exploratory combinatorial optimization with reinforcement learning. In *Proceedings of the AAAI conference on artificial intelligence*, volume 34, pages 3243–3250, 2020.
- [BGJR88] F. Barahona, M. Grötschel, M. Jünger, and G. Reinelt. An application of combinatorial optimization to statistical physics and circuit layout design. *Operations Research*, 36(3):493–513, 1988.

- [BH13] Una Benlic and Jin-Kao Hao. Breakout local search for the max-cut problem. *Engineering Applications of Artificial Intelligence*, 26(3):1162–1173, 2013.
- [BP21] Daniel Beaulieu and Anh Pham. Max-cut clustering utilizing warm-start qaoa and ibm runtime, 2021.
- [BPL22] Thomas D Barrett, Christopher WF Parsonson, and Alexandre Laterre. Learning to solve combinatorial graph partitioning problems via efficient exploration. *arXiv preprint arXiv:2205.14105*, 2022.
- [Bré79] Daniel Bréaz. New methods to color the vertices of a graph. *Communications of the ACM*, 22(4):251–256, 1979.
- [BRS12] Boaz Barak, Prasad Raghavendra, and David Steurer. Rounding semidefinite programming hierarchies via global correlation. In *Proceedings of the 44th ACM Symposium on Theory of Computing (STOC)*, pages 31–40, 2012.
- [CCF18] Y. Chen, C. Cheng, and J. Fan. Asymmetry helps: Eigenvalue and eigenvector analyses of asymmetrically perturbed low-rank matrices. *arXiv preprint arXiv:1811.12804*, 2018.
- [CRS98] Jun-Dong Cho, Salil Raje, and Majid Sarrafzadeh. Fast approximation algorithms on MAX-CUT,  $k$ -coloring, and  $k$ -color ordering for VLSI applications. *IEEE Transactions on Computers*, 47(11):1253–1266, 1998.
- [DH11] Timothy A Davis and Yifan Hu. The university of florida sparse matrix collection. *ACM Transactions on Mathematical Software (TOMS)*, 38(1):1–25, 2011.
- [dKPW04] Etienne de Klerk, Dmitrii V Pasechnik, and Joost P Warners. On approximate graph colouring and MAX- $k$ -CUT algorithms based on the  $\theta$ -function. *Journal of Combinatorial Optimization*, 8(3):267–294, 2004.
- [DL94] M. Deza and M. Laurent. Applications of cut polyhedra - II. *Journal of Computational and Applied Mathematics*, 55(2):217–247, 1994.
- [FGG14] Edward Farhi, Jeffrey Goldstone, and Sam Gutmann. A quantum approximate optimization algorithm. *arXiv preprint arXiv:1411.4028*, 2014.
- [FHL<sup>+</sup>19] Damir Ferizovic, Demian Hesse, Sebastian Lamm, Matthias Mnich, Christian Schulz, and Darren Strash. Engineering kernelization for maximum cut, 2019.
- [FJ97] Alan Frieze and Mark Jerrum. Improved approximation algorithms for MAX  $k$ -CUT and MAX BISECTION. *Algorithmica*, 18(1):67–81, 1997.
- [FK99] Alan M. Frieze and Ravi Kannan. Quick approximation to matrices and applications. *Combinatorica*, 19(2):175–220, 1999.
- [GD24] Etienne Granet and Henrik Dreyer. Benchmarking a heuristic floquet adiabatic algorithm for the max-cut problem, 2024.
- [GGH24] Olivier Goudet, Adrien Goëffon, and Jin-Kao Hao. A large population island framework for the unconstrained binary quadratic problem. *Computers & Operations Research*, 168:106684, 2024.
- [GJG18] Jihong Gui, Zhipeng Jiang, and Suixiang Gao. Pci planning based on binary quadratic programming in lte/lte-a networks. *IEEE Access*, 7:203–214, 2018.
- [GPI13] F. Gieseke, T. Pahikkala, and C. Igel. Polynomial runtime bounds for fixed-rank unsupervised least-squares classification. In *Asian Conference on Machine Learning*, pages 62–71, 2013.
- [GT15] Shayan Oveis Gharan and Luca Trevisan. A new regularity lemma and faster approximation algorithms for low threshold rank graphs. *Theory of Computing*, 11(9):209–262, 2015.

- [GW95] M. Goemans and D. Williamson. Improved approximation algorithms for maximum cut and satisfiability problems using semidefinite programming. *Journal of the ACM (JACM)*, 42(6):1115–1145, 1995.
- [GW01] Michel X Goemans and David Williamson. Approximation algorithms for MAX-3-CUT and other problems via complex semidefinite programming. In *Proceedings of the thirty-third annual ACM symposium on Theory of computing*, pages 443–452, 2001.
- [Har96] A. Hartmann. Cluster-exact approximation of spin glass groundstates. *Physica A: Statistical Mechanics and its Applications*, 224(3-4):480–488, 1996.
- [HSS08] Aric A. Hagberg, Daniel A. Schult, and Pieter J. Swart. Exploring network structure, dynamics, and function using networkx. In Gaël Varoquaux, Travis Vaught, and Jarrod Millman, editors, *Proceedings of the 7th Python in Science Conference*, pages 11 – 15, Pasadena, CA USA, 2008.
- [JAMS91] David S Johnson, Cecilia R Aragon, Lyle A McGeoch, and Catherine Schevon. Optimization by simulated annealing: an experimental evaluation; part II, graph coloring and number partitioning. *Operations research*, 39(3):378–406, 1991.
- [Kar72] R. Karp. Reducibility among combinatorial problems. In *Complexity of computer computations*, pages 85–103. Springer, 1972.
- [KDZ<sup>+</sup>17] Elias Khalil, Hanjun Dai, Yuyu Zhang, Bistra Dilkina, and Le Song. Learning combinatorial optimization algorithms over graphs. *Advances in neural information processing systems*, 30, 2017.
- [KK11] A. Kyrillidis and G. Karystinos. Rank-deficient quadratic-form maximization over  $m$ -phase alphabet: Polynomial-complexity solvability and algorithmic developments. In *2011 IEEE International Conference on Acoustics, Speech and Signal Processing (ICASSP)*, pages 3856–3859. IEEE, 2011.
- [KK14] A. Kyrillidis and G. Karystinos. Fixed-rank Rayleigh quotient maximization by an MPSK sequence. *IEEE Transactions on Communications*, 62(3):961–975, 2014.
- [KKMO07] Subhash Khot, Guy Kindler, Elchanan Mossel, and Ryan O’Donnell. Optimal inapproximability results for MaxCUT and other 2-variable CSPs? *SIAM Journal on Computing*, 37(1):319–357, 2007.
- [KL06] G. Karystinos and A. Liavas. Efficient computation of the binary vector that maximizes a rank-3 quadratic form. In *Proc. 2006 Allerton Conf. Commun., Control, and Computing*, pages 1286–1291, 2006.
- [KL20] Nikolaos Karalias and Andreas Loukas. Erdos goes neural: an unsupervised learning framework for combinatorial optimization on graphs. *Advances in Neural Information Processing Systems*, 33:6659–6672, 2020.
- [LSS15] Sebastian Lamm, Peter Sanders, and Christian Schulz. Graph partitioning for independent sets. In *International Symposium on Experimental Algorithms*, pages 68–81. Springer, 2015.
- [LZ13] Geng Lin and Wenxing Zhu. An efficient memetic algorithm for themax-bisection problem. *IEEE Transactions on Computers*, 63(6):1365–1376, 2013.
- [MH17] Fuda Ma and Jin-Kao Hao. A multiple search operator heuristic for the max-k-cut problem. *Annals of Operations Research*, 248(1):365–403, 2017.
- [MHA19] Anirudha Majumdar, Georgina Hall, and Amir Ali Ahmadi. A survey of recent scalability improvements for semidefinite programming with applications in machine learning, control, and robotics, 2019.

- [MMMO17] S. Mei, T. Misiakiewicz, A. Montanari, and R. Oliveira. Solving SDPs for synchronization and MaxCut problems via the Grothendieck inequality. In *Conference on Learning Theory*, pages 1476–1515, 2017.
- [MNW<sup>+</sup>18] Philipp Moritz, Robert Nishihara, Stephanie Wang, Alexey Tumanov, Richard Liaw, Eric Liang, Melih Elibol, Zongheng Yang, William Paul, Michael I Jordan, et al. Ray: A distributed framework for emerging {AI} applications. In *13th USENIX symposium on operating systems design and implementation (OSDI 18)*, pages 561–577, 2018.
- [New18] Alantha Newman. A new approximation guarantee for the MAX  $k$ -CUT problem. *Mathematical Programming*, 172(1–2):583–609, 2018.
- [Pat98] G. Pataki. On the rank of extreme matrices in semidefinite programs and the multiplicity of optimal eigenvalues. *Mathematics of operations research*, 23(2):339–358, 1998.
- [PJ16] LI Panxing and WANG Jing. Pci planning method based on genetic algorithm in lte network. *Telecommunications Science*, 32(3):2016082, 2016.
- [QXW<sup>+</sup>24] Yeqing Qiu, Ye Xue, Akang Wang, Yiheng Wang, Qingjiang Shi, and Zhi-Quan Luo. Ros: A gnn-based relax-optimize-and-sample framework for max-k-cut problems. *arXiv preprint arXiv:2412.05146*, 2024.
- [SBK22] Martin JA Schuetz, J Kyle Brubaker, and Helmut G Katzgraber. Combinatorial optimization with physics-inspired graph neural networks. *Nature Machine Intelligence*, 4(4):367–377, 2022.
- [SGS15] VP Shylo, Fred Glover, and IV Sergienko. Teams of global equilibrium search algorithms for solving the weighted maximum cut problem in parallel. *Cybernetics and Systems Analysis*, 51(1):16–24, 2015.
- [Sin11] A. Singer. Angular synchronization by eigenvectors and semidefinite programming. *Applied and computational harmonic analysis*, 30(1):20–36, 2011.
- [SM00] J. Shi and J. Malik. Normalized cuts and image segmentation. *IEEE Transactions on pattern analysis and machine intelligence*, 22(8):888–905, 2000.
- [Sot15] José A Soto. Improved analysis of a max-cut algorithm based on spectral partitioning. *SIAM Journal on Discrete Mathematics*, 29(1):259–268, 2015.
- [SSR12] VP Shylo, OV Shylo, and VA Roschyn. Solving weighted max-cut problem by global equilibrium search. *Cybernetics and Systems Analysis*, 48(4):563–567, 2012.
- [TKLG22] Jan Tönshoff, Berke Kisin, Jakob Lindner, and Martin Grohe. One model, any csp: graph neural networks as fast global search heuristics for constraint satisfaction. *arXiv preprint arXiv:2208.10227*, 2022.
- [Ver18] Roman Vershynin. *High-dimensional probability: An introduction with applications in data science*, volume 47. Cambridge university press, 2018.
- [Vit81] Paul MB Vitanyi. How well can a graph be  $n$ -colored? *Discrete mathematics*, 34(1):69–80, 1981.
- [Wed72] P. Wedin. Perturbation bounds in connection with singular value decomposition. *BIT Numerical Mathematics*, 12(1):99–111, 1972.
- [WH12] Qinghua Wu and Jin-Kao Hao. A memetic approach for the max-cut problem. In *International Conference on Parallel Problem Solving from Nature*, pages 297–306. Springer, 2012.
- [WJC13] J. Wang, T. Jebara, and S.-F. Chang. Semi-supervised learning using greedy MaxCut. *Journal of Machine Learning Research*, 14(Mar):771–800, 2013.

- [YBV19] Weichi Yao, Afonso S Bandeira, and Soledad Villar. Experimental performance of graph neural networks on random instances of max-cut. In *Wavelets and Sparsity XVIII*, volume 11138, pages 242–251. SPIE, 2019.
- [Ye03] Yinyu Ye. The gset dataset, 2003.

## A Derivation of Complex Ternary Quadratic Form for Max-3-Cut

We derive the complex ternary quadratic formulation of MAX-3-CUT. Let  $G = (V, E)$  be an undirected graph with vertex set  $V = \{1, 2, \dots, p\}$  and edge set  $E$ . Let  $w : E \rightarrow \mathbb{R}^+$  be a weight function assigning positive weights to edges. The Max-3-CUT problem seeks a partition of  $\mathbf{V}$  into 3 disjoint sets  $\mathcal{S}_1, \mathcal{S}_2, \mathcal{S}_3$  such that the sum of weights of edges crossing between different sets is maximized:

$$\max_{\mathcal{S}_1, \mathcal{S}_2, \mathcal{S}_3} \sum_{i \in \mathcal{S}_1, \ell \in \mathcal{S}_2} w_{i\ell} + \sum_{i \in \mathcal{S}_1, \ell \in \mathcal{S}_3} w_{i\ell} + \sum_{i \in \mathcal{S}_2, \ell \in \mathcal{S}_3} w_{i\ell}. \quad (20)$$

### A.0.1 Complex Encoding of Partitions.

To reformulate the Max-3-CUT problem in the complex domain, we encode the partitioning of vertices using complex cube roots of unity. Let  $\omega_3 = e^{j2\pi/3}$  be the primitive cube root of unity. Then, each vertex  $i$  is assigned a value  $z_i \in \mathcal{A}_3 := \{1, \omega_3, \omega_3^2\}$ , where:

$$\begin{aligned} z_i = 1 &\Rightarrow i \in \mathcal{S}_1 \\ z_i = \omega_3 &= e^{j2\pi/3} \Rightarrow i \in \mathcal{S}_2 \\ z_i = \omega_3^2 &= e^{4\pi j/3} \Rightarrow i \in \mathcal{S}_3 \end{aligned}$$

A property we exploit is that for any two complex roots of unity  $\alpha$  and  $\beta$ :

$$\alpha \neq \beta \Rightarrow \operatorname{Re}(\alpha\bar{\beta}) = \cos\left(\frac{2\pi}{3}|p-q|\right)$$

where  $\alpha = \omega_3^{p-1}$  and  $\beta = \omega_3^{q-1}$  for some  $p, q \in \{1, 2, 3\}$ . Then, this gives:

$$\operatorname{Re}(z_i\bar{z}_\ell) = \begin{cases} 1, & \text{if } i \text{ \& } \ell \text{ in same partition;} \\ \cos(\frac{2\pi}{3}) = -\frac{1}{2}, & \text{otherwise.} \end{cases}$$

### A.0.2 Reformulation as a Quadratic Optimization.

Using the above complex encoding, we can reformulate the Max-3-CUT problem as a quadratic optimization problem. The objective function can be written as:

$$\max_{\mathbf{z} \in \mathcal{A}_3^p} \sum_{(i,\ell) \in E} w_{i\ell} \cdot (1 - \operatorname{Re}(z_i\bar{z}_\ell)) \quad (21)$$

Let us verify that this objective function correctly captures the MAX-3-CUT problem:

- If vertices  $i$  and  $\ell$  are in the same partition, then  $z_i = z_\ell$ , which means  $z_i\bar{z}_\ell = |z_i|^2 = 1$ , so  $\operatorname{Re}(z_i\bar{z}_\ell) = 1$ . Thus, the contribution of this edge is  $w_{i\ell} \cdot (1 - 1) = 0$ .
- If vertices  $i$  and  $\ell$  are in different partitions, then  $z_i \neq z_\ell$ , and they correspond to different 3-rd roots of unity. In this case,  $\operatorname{Re}(z_i\bar{z}_\ell) = \cos(\frac{2\pi|p-q|}{3})$ , where  $p$  and  $q$  are the respective partitions. Since  $K = 3$ , the contribution of this edge to the objective is  $w_{i\ell} \cdot (1 - \cos(\frac{2\pi|p-q|}{3})) = w_{i\ell} \cdot (1 - (-1/2)) = \frac{3}{2}w_{i\ell}$ .

### A.0.3 Generalized Complex Laplacian Formulation.

To further develop our approach, we introduce the generalized complex Laplacian matrix. Let  $\mathbf{W} = \{w_{i\ell}\}_{i,\ell=1}^p$  be the weighted adjacency matrix of graph  $G$ , and let  $\mathbf{D} = \operatorname{diag}(d_1, d_2, \dots, d_n)$  be the diagonal matrix of weighted degrees, where  $d_i = \sum_{\ell: (i,\ell) \in E} w_{i\ell}$ . The standard graph Laplacian is defined as

$\mathbf{Q} = \mathbf{D} - \mathbf{W}$ . Using the properties of the Laplacian, we can express the objective function above as:

$$\begin{aligned}
& \sum_{(i,\ell) \in E} w_{i\ell} \cdot (1 - \operatorname{Re}(z_i \bar{z}_\ell)) \\
&= \sum_{(i,\ell) \in E} w_{i\ell} - \sum_{(i,\ell) \in E} w_{i\ell} \cdot \operatorname{Re}(z_i \bar{z}_\ell) \\
&= \sum_{i \in V} d_i - \operatorname{Re} \left( \sum_{(i,\ell) \in E} w_{i\ell} \cdot z_i \bar{z}_\ell \right) \\
&= \operatorname{tr}(\mathbf{D}) - \operatorname{Re}(\mathbf{z}^\dagger \mathbf{W} \mathbf{z}) \\
&= \operatorname{Re}(\mathbf{z}^\dagger \mathbf{Q} \mathbf{z}).
\end{aligned}$$

Thus, the Max-3-CUT problem can be formulated as:

$$\text{OPT-Q} := \max_{\mathbf{z} \in \mathcal{A}_3^p} \mathbf{z}^\dagger \mathbf{Q} \mathbf{z}.$$

## B Proof of Theorem 3

**Theorem 3.** *Let  $\mathbf{Q}_r \in \mathbb{C}^{n \times n}$  be a rank- $r$ , positive semi-definite matrix. Algorithm 2 solves the discrete quadratic maximization problem (2) with objective matrix  $\mathbf{Q}_r$  in  $\mathcal{O}(rn^{2r+1})$  time.*

*Proof.* This proof combines the information of the auxiliary results given in Appendix C.

### Proof of Time Complexity.

In Theorem 15, we prove that the algorithm enumerates  $\mathcal{O}(rn^{2r-1})$  candidates. Evaluating each candidate requires computing the corresponding quadratic form in  $\mathcal{O}(n^2)$  time. The overall time complexity is therefore  $\mathcal{O}(rn^{2r+1})$ .

### Proof of Correctness

We show that the candidate set  $\mathcal{S}(\mathbf{V})$  enumerated by the algorithm contains the global maximizer.

*Step 1: Reformulation as double maximization.* By the Cauchy-Schwarz argument (Lemma C.1 and the subsequent discussion):

$$\max_{\mathbf{z} \in \mathcal{A}_K^n} \|\mathbf{V}^\dagger \mathbf{z}\|_2 = \max_{\phi \in \mathcal{H}_r} \max_{\mathbf{z} \in \mathcal{A}_K^n} \Re\{\mathbf{z}^\dagger \mathbf{V} \mathbf{c}(\phi)\} = \max_{\phi \in \mathcal{H}_r} \sum_{i=1}^n \max_{z_i \in \mathcal{A}_K} \Re\{z_i^* \mathbf{V}_{i,:} \mathbf{c}(\phi)\}. \quad (22)$$

The second equality holds because, for fixed  $\phi$ , the coordinates  $z_i$  can be optimized independently.

*Step 2: Decision function is piecewise constant.* For fixed  $\phi$ , the optimal  $z_i$  is determined by the decision rule:

$$d_i(\mathbf{V}; \phi) = \arg \max_{z \in \mathcal{A}_K} \Re\{z^* \mathbf{V}_{i,:} \mathbf{c}(\phi)\}. \quad (23)$$

Let  $\alpha_i(\phi) = \mathbf{V}_{i,:} \mathbf{c}(\phi)$ . The optimal  $z_i$  is the element of  $\mathcal{A}_K$  whose phase is closest to  $\arg(\alpha_i(\phi))$ . As  $\phi$  varies, the phase of  $\alpha_i$  varies continuously, and  $d_i$  changes only when  $\arg(\alpha_i)$  crosses a boundary angle  $\vartheta_m$ .

*Step 3: Hypersurfaces partition  $\mathcal{H}_r$  into cells.* The  $B_K n$  hypersurfaces  $\{\mathcal{H}(\tilde{\mathbf{V}}_{j,:})\}_{j=1}^{B_K n}$  partition  $\mathcal{H}_r$  into cells. Within each cell, the decision function  $\mathbf{d}(\mathbf{V}; \phi)$  is constant. The objective  $\sum_i \max_{z_i} \Re\{z_i^* \alpha_i(\phi)\}$  is continuous in  $\phi$ , so the global maximum is attained either:

- (a) At a vertex of the arrangement (intersection of  $2r - 1$  hypersurfaces), or
- (b) On the boundary of  $\mathcal{H}_r$ .

*Step 4: Enumeration of interior vertices.* The main loop of Algorithm 2 enumerates all valid index sets  $\mathcal{I} \subset [B_K n]$  with  $|\mathcal{I}| = 2r - 1$  and checks if  $\operatorname{rank}(\tilde{\mathbf{V}}_{\mathcal{I},:}) = 2r - 1$ . For each such  $\mathcal{I}$ , it computes the vertex  $\phi(\mathbf{V}; \mathcal{I})$ , applies the decision rule to obtain a candidate  $\mathbf{z}_{\mathcal{I}}$ , and evaluates the objective.

By Lemma C.19, this enumeration covers all cells whose "leading vertex" (the vertex with minimal  $\phi_{2r-1}$ ) lies in the interior of  $\mathcal{H}_r$ .

*Step 5: Recursive handling of boundary cases.* Cells touching the boundary  $\phi_{2r-1} = -\pi/K$  or  $\phi_{2r-1} = \pi/K$  are not captured by interior vertices. However:

- By Corollary C.16, candidates from  $\phi_{2r-1} = -\pi/K$  are phase rotations of candidates from elsewhere, so no loss occurs.
- Candidates from  $\phi_{2r-2} = \pm\pi/2$  (with arbitrary  $\phi_{2r-1}$ ) correspond to the rank- $(r-1)$  problem on  $\mathbf{V}_{:,1:r-1}$ . The recursive call handles these.

Overall, the boundary of the hypercube  $\mathcal{H}_r$  consists of faces where one angular coordinate is fixed at its extreme value. When this occurs, one degree of freedom in the auxiliary vector  $\mathbf{c}(\boldsymbol{\phi})$  is eliminated: either a magnitude allocation coordinate ( $\phi_j = \pm\pi/2$ ) becomes extremal, or the final phase coordinate ( $\phi_{2r-1} = \pm\pi/K$ ) is fixed. In both cases, the effective optimization over the remaining  $2(r-1) - 1$  free parameters reduces to a rank- $(r-1)$  subproblem, which is solved by the recursive call in Algorithm 2. This is proven in [KK14].

This reduction is independent of the alphabet size  $K$ . The specific boundary values differ with  $K$  (e.g.,  $\pm\pi/K$  for the phase coordinate), but the mechanism (fixing one coordinate eliminates one degree of freedom) is purely structural. Combined with the interior vertex enumeration, this ensures that the candidate set contains the global optimizer for any rank- $r$  PSD matrix and any  $K \geq 2$ .

*Step 6: Completeness of candidate set.* Combining Steps 4 and 5, every cell of the arrangement is associated with at least one candidate in  $\mathcal{S}(\mathbf{V})$ . Since the global maximizer lies in some cell, it is in  $\mathcal{S}(\mathbf{V})$ .

*Step 7: Evaluation and selection.* The algorithm evaluates the objective for all candidates and returns the best one. Since the global maximizer is in  $\mathcal{S}(\mathbf{V})$ , the returned  $\mathbf{z}^*$  achieves the maximum.  $\square$   $\square$

## C Auxiliary Results for the Proof of Theorem 3

This appendix provides a complete theoretical treatment of the discrete quadratic maximization problem (2) for general alphabet size  $K \geq 2$ , encompassing both even and odd values. We establish the decision boundary structure, construct the augmented matrix, prove the candidate set characterization, and demonstrate algorithm correctness. The facts, lemmas and corollaries throughout this section serve as key pieces in the proof of Theorem 3, given in Appendix B.

### C.1 Preliminaries and Notation

We consider the discrete quadratic maximization problem:

$$\text{OPT-Q} := \max_{\mathbf{z} \in \mathcal{A}_K^n} \mathbf{z}^\dagger \mathbf{Q} \mathbf{z}, \quad (24)$$

where  $\mathbf{Q} \in \mathbb{C}^{n \times n}$  is Hermitian and positive semi-definite, and  $\mathcal{A}_K$  denotes the  $K$ -th roots of unity:

$$\mathcal{A}_K = \left\{ \exp\left(\frac{2\pi i k}{K}\right) : k \in \{0, 1, \dots, K-1\} \right\}. \quad (25)$$

Since  $\mathbf{Q}$  is PSD with rank  $r$ , we may write  $\mathbf{Q} = \mathbf{V} \mathbf{V}^\dagger$  for some  $\mathbf{V} \in \mathbb{C}^{n \times r}$ . The objective becomes:

$$\mathbf{z}^\dagger \mathbf{Q} \mathbf{z} = \mathbf{z}^\dagger \mathbf{V} \mathbf{V}^\dagger \mathbf{z} = \|\mathbf{V}^\dagger \mathbf{z}\|_2^2. \quad (26)$$

We parameterize the unit sphere in  $\mathbb{C}^r$  using hyperpolar coordinates. Let  $\boldsymbol{\phi} = (\phi_1, \dots, \phi_{2r-1})^\top$  with  $\phi_i \in (-\frac{\pi}{2}, \frac{\pi}{2}]$  for  $i = 1, \dots, 2r-2$  and  $\phi_{2r-1} \in (-\frac{\pi}{K}, \frac{\pi}{K}]$ . Define the real hyperpolar vector  $\tilde{\mathbf{c}}(\boldsymbol{\phi}) \in \mathbb{R}^{2r}$  by:

$$\tilde{\mathbf{c}}(\boldsymbol{\phi}) = \begin{bmatrix} \sin \phi_1 \\ \cos \phi_1 \sin \phi_2 \\ \cos \phi_1 \cos \phi_2 \sin \phi_3 \\ \vdots \\ \left( \prod_{i=1}^{2r-2} \cos \phi_i \right) \sin \phi_{2r-1} \\ \left( \prod_{i=1}^{2r-2} \cos \phi_i \right) \cos \phi_{2r-1} \end{bmatrix}, \quad (27)$$

and the complex unit vector  $\mathbf{c}(\boldsymbol{\phi}) \in \mathbb{C}^r$  by:

$$\mathbf{c}(\boldsymbol{\phi}) = \tilde{\mathbf{c}}_{2:2:2r}(\boldsymbol{\phi}) + \hat{i} \tilde{\mathbf{c}}_{1:2:2r-1}(\boldsymbol{\phi}), \quad (28)$$

where subscript notation  $\tilde{\mathbf{c}}_{a:b:c}$  denotes elements at indices  $a, a+b, a+2b, \dots$  up to  $c$ .

**Lemma C.1** (Unit Norm Property). *For all  $\boldsymbol{\phi}$  in the domain,  $\|\tilde{\mathbf{c}}(\boldsymbol{\phi})\|_2 = \|\mathbf{c}(\boldsymbol{\phi})\|_2 = 1$ .*

*Proof.* Direct calculation shows  $\|\tilde{\mathbf{c}}(\boldsymbol{\phi})\|_2^2 = \sin^2 \phi_1 + \cos^2 \phi_1 (\sin^2 \phi_2 + \cos^2 \phi_2 (\dots)) = 1$  by repeated application of the identity  $\sin^2 \theta + \cos^2 \theta = 1$ . The complex norm follows since  $\|\mathbf{c}(\boldsymbol{\phi})\|_2^2 = \|\tilde{\mathbf{c}}(\boldsymbol{\phi})\|_2^2$ .  $\square$   $\square$

Finally, define the hypercube:

$$\mathcal{H}_r := \left(-\frac{\pi}{2}, \frac{\pi}{2}\right]^{2r-2} \times \left(-\frac{\pi}{K}, \frac{\pi}{K}\right]. \quad (29)$$

## C.2 Decision Boundary Structure for General $K$

The decision boundaries determine where the optimal symbol assignment for a coordinate changes as the auxiliary angle vector  $\boldsymbol{\phi}$  varies.

**Definition C.2** (Boundary Angles). *For alphabet size  $K \geq 2$ , the boundary angles are:*

$$\vartheta_m = \frac{\pi(2m+1)}{K}, \quad m \in \{0, 1, \dots, K-1\}. \quad (30)$$

*These angles bisect adjacent symbol phases in  $\mathcal{A}_K$ : the boundary at  $\vartheta_m$  separates the sectors corresponding to symbols  $e^{2\pi i m/K}$  and  $e^{2\pi i (m+1)/K}$ .*

**Definition C.3** (Decision Boundary). *For coordinate  $i \in [n]$  and boundary index  $m \in \{0, \dots, K-1\}$ , the decision boundary  $\mathcal{B}_{i,m}$  is the set of angle vectors  $\boldsymbol{\phi} \in \mathcal{H}_r$  such that  $\mathbf{V}_{i,:} \mathbf{c}(\boldsymbol{\phi})$  lies on the ray at angle  $\vartheta_m$  from the origin:*

$$\mathcal{B}_{i,m} = \{ \boldsymbol{\phi} \in \mathcal{H}_r : \mathbf{V}_{i,:} \mathbf{c}(\boldsymbol{\phi}) = A e^{i\vartheta_m} \text{ for some } A \in \mathbb{R} \}. \quad (31)$$

The condition  $\mathbf{V}_{i,:} \mathbf{c}(\boldsymbol{\phi}) = A e^{i\vartheta_m}$  for real  $A$  is equivalent to requiring that  $e^{-i\vartheta_m} \mathbf{V}_{i,:} \mathbf{c}(\boldsymbol{\phi})$  is real, i.e.:

$$\Im \{ e^{-i\vartheta_m} \mathbf{V}_{i,:} \mathbf{c}(\boldsymbol{\phi}) \} = 0. \quad (32)$$

**Lemma C.4** (Antipodal Boundary Equivalence). *The decision boundaries at angles  $\vartheta_m$  and  $\vartheta_m + \pi$  define the same hyperplane in  $\mathcal{H}_r$  if and only if  $K$  is even.*

*Proof.* The boundary condition (32) at angle  $\vartheta_m + \pi$  is:

$$\Im \{ e^{-i(\vartheta_m + \pi)} \mathbf{V}_{i,:} \mathbf{c}(\boldsymbol{\phi}) \} = \Im \{ -e^{-i\vartheta_m} \mathbf{V}_{i,:} \mathbf{c}(\boldsymbol{\phi}) \} = -\Im \{ e^{-i\vartheta_m} \mathbf{V}_{i,:} \mathbf{c}(\boldsymbol{\phi}) \}. \quad (33)$$

Thus, the condition  $\Im \{ e^{-i(\vartheta_m + \pi)} \mathbf{V}_{i,:} \mathbf{c}(\boldsymbol{\phi}) \} = 0$  is equivalent to  $\Im \{ e^{-i\vartheta_m} \mathbf{V}_{i,:} \mathbf{c}(\boldsymbol{\phi}) \} = 0$ , meaning both boundary conditions define the same hyperplane.

For this to result in a reduction of the number of distinct boundaries, we need  $\vartheta_m + \pi = \vartheta_{m'}$  for some  $m' \in \{0, \dots, K-1\}$ . We have:

$$\vartheta_m + \pi = \frac{\pi(2m+1)}{K} + \pi = \frac{\pi(2m+1+K)}{K} = \frac{\pi(2(m+K/2)+1)}{K}. \quad (34)$$

This equals  $\vartheta_{m+K/2}$  if and only if  $K/2$  is an integer, i.e., if and only if  $K$  is even.

When  $K$  is even, each boundary angle  $\vartheta_m$  for  $m \in \{0, \dots, K/2-1\}$  is paired with  $\vartheta_{m+K/2}$ , and they define the same hyperplane. When  $K$  is odd, no two boundary angles differ by exactly  $\pi$ , so all  $K$  boundaries are distinct.  $\square$   $\square$

**Definition C.5** (Effective Boundary Count). *The number of distinct decision boundaries per coordinate is:*

$$B_K = \begin{cases} K/2 & \text{if } K \text{ is even,} \\ K & \text{if } K \text{ is odd.} \end{cases} \quad (35)$$

**Example 6** ( $K = 2$ : Binary Case). For  $K = 2$ , we have  $\vartheta_0 = \pi/2$  and  $\vartheta_1 = 3\pi/2$ . Since  $\vartheta_1 = \vartheta_0 + \pi$ , these define the same hyperplane. Thus  $B_2 = 1$  boundary per coordinate, corresponding to the real axis separating  $+1$  from  $-1$ .

**Example 7** ( $K = 3$ : Ternary Case). For  $K = 3$ , we have  $\vartheta_0 = \pi/3$ ,  $\vartheta_1 = \pi$ , and  $\vartheta_2 = 5\pi/3$ . Checking for antipodal pairs:

- $\vartheta_0 + \pi = 4\pi/3 \neq \vartheta_m$  for any  $m$
- $\vartheta_1 + \pi = 2\pi \equiv 0 \neq \vartheta_m$  for any  $m$
- $\vartheta_2 + \pi = 8\pi/3 = 2\pi/3 \pmod{2\pi} \neq \vartheta_m$  for any  $m$

All three boundaries are distinct, so  $B_3 = 3$ .

**Example 8** ( $K = 4$ : Quaternary Case). For  $K = 4$ , we have  $\vartheta_0 = \pi/4$ ,  $\vartheta_1 = 3\pi/4$ ,  $\vartheta_2 = 5\pi/4$ ,  $\vartheta_3 = 7\pi/4$ . The pairs  $(\vartheta_0, \vartheta_2)$  and  $(\vartheta_1, \vartheta_3)$  differ by  $\pi$ , giving  $B_4 = 2$  distinct boundaries.

### C.3 Augmented Matrix Construction

We now construct the real augmented matrix that encodes all decision boundaries for general  $K$ .

**Definition C.6** (Rotation Factors). *For general  $K \geq 2$ , define the rotation factors as:*

$$\rho_m = e^{-i\vartheta_m} = e^{-i\pi(2m+1)/K}, \quad m \in \mathcal{M}_K, \quad (36)$$

where the index set  $\mathcal{M}_K$  is:

$$\mathcal{M}_K = \begin{cases} \{0, 1, \dots, K/2-1\} & \text{if } K \text{ is even,} \\ \{0, 1, \dots, K-1\} & \text{if } K \text{ is odd.} \end{cases} \quad (37)$$

**Definition C.7** (Rotated Factor Matrix). *The rotated factor matrix  $\hat{\mathbf{V}} \in \mathbb{C}^{B_K n \times r}$  is:*

$$\hat{\mathbf{V}} = \begin{bmatrix} \rho_0 \\ \rho_1 \\ \vdots \\ \rho_{B_K-1} \end{bmatrix} \otimes \mathbf{V} = \begin{bmatrix} \rho_0 \mathbf{V} \\ \rho_1 \mathbf{V} \\ \vdots \\ \rho_{B_K-1} \mathbf{V} \end{bmatrix}. \quad (38)$$

The decision boundary condition (32) for all coordinates and all relevant boundary angles can be written as:

$$\Im \left\{ \hat{\mathbf{V}} \mathbf{c}(\phi) \right\} = \mathbf{0}_{B_K n}. \quad (39)$$

**Definition C.8** (Real Augmented Matrix). *The real augmented matrix  $\tilde{\mathbf{V}} \in \mathbb{R}^{B_K n \times 2r}$  is constructed by separating real and imaginary parts:*

$$\tilde{\mathbf{V}} = [\Re\{\hat{\mathbf{V}}\} \quad \Im\{\hat{\mathbf{V}}\}]. \quad (40)$$

*Equivalently, using the column interleaving that maps the complex product to a real inner product:*

$$\tilde{\mathbf{V}}_{:,1:2:2r-1} = \Re\{\hat{\mathbf{V}}\}, \quad \tilde{\mathbf{V}}_{:,2:2:2r} = \Im\{\hat{\mathbf{V}}\}. \quad (41)$$

**Lemma C.9** (Boundary Reformulation). *The decision boundary conditions are equivalent to the linear system:*

$$\tilde{\mathbf{V}}\tilde{\mathbf{c}}(\phi) = \mathbf{0}_{B_K n}. \quad (42)$$

*Proof.* For any  $\mathbf{a} \in \mathbb{C}^r$ , we have:

$$\Im\{\mathbf{a}^\top \mathbf{c}(\phi)\} = \Im\left\{\sum_{j=1}^r a_j c_j(\phi)\right\} \quad (43)$$

$$= \sum_{j=1}^r (\Re\{a_j\}\Im\{c_j(\phi)\} + \Im\{a_j\}\Re\{c_j(\phi)\}) \quad (44)$$

$$= [\Re\{\mathbf{a}\}^\top \quad \Im\{\mathbf{a}\}^\top] \begin{bmatrix} \Im\{\mathbf{c}(\phi)\} \\ \Re\{\mathbf{c}(\phi)\} \end{bmatrix}. \quad (45)$$

By the construction (28),  $\Im\{\mathbf{c}(\phi)\} = \tilde{\mathbf{c}}_{1:2:2r-1}(\phi)$  and  $\Re\{\mathbf{c}(\phi)\} = \tilde{\mathbf{c}}_{2:2:2r}(\phi)$ . With the column arrangement in (40), this gives  $\Im\{\tilde{\mathbf{V}}\mathbf{c}(\phi)\} = \tilde{\mathbf{V}}\tilde{\mathbf{c}}(\phi)$ .  $\square$   $\square$

**Definition C.10** (Coordinate Groups). *For each coordinate  $i \in [n]$ , the coordinate group  $\mathcal{G}^{(i)} \in \mathbb{R}^{B_K \times 2r}$  consists of the  $B_K$  rows of  $\tilde{\mathbf{V}}$  corresponding to coordinate  $i$ :*

$$\mathcal{G}^{(i)} = \begin{bmatrix} \tilde{\mathbf{V}}_{i,:} \\ \tilde{\mathbf{V}}_{i+n,:} \\ \vdots \\ \tilde{\mathbf{V}}_{i+(B_K-1)n,:} \end{bmatrix}. \quad (46)$$

*Each row of  $\mathcal{G}^{(i)}$  corresponds to a different decision boundary for coordinate  $i$ .*

**Remark 9** (Specialization to Even  $K$ ). *For even  $K$ , the construction reduces to that in the foundational paper [KK11] with  $M \equiv K$  and  $M/2 = B_K$  rotation factors. The matrix dimensions are  $\tilde{\mathbf{V}} \in \mathbb{R}^{nK/2 \times 2r}$ .*

**Remark 10** (Specialization to  $K = 3$ ). *For  $K = 3$ , we have  $B_3 = 3$  with rotation factors:*

$$\rho_0 = e^{-i\pi/3}, \quad \rho_1 = e^{-i\pi} = -1, \quad \rho_2 = e^{-i5\pi/3}. \quad (47)$$

*The rotated matrix is:*

$$\hat{\mathbf{V}}_{3n \times r} = \begin{bmatrix} e^{-i\pi/3}\mathbf{V} \\ -\mathbf{V} \\ e^{-i5\pi/3}\mathbf{V} \end{bmatrix}, \quad (48)$$

*and  $\tilde{\mathbf{V}} \in \mathbb{R}^{3n \times 2r}$ .*

## C.4 Intersection Properties and Group Structure

We now establish the key structural property that all hypersurfaces from the same coordinate group intersect at a common lower-dimensional manifold.

**Definition C.11** (Hypersurface). *For row index  $j \in [B_K n]$  of  $\tilde{\mathbf{V}}$ , the hypersurface  $\mathcal{H}(\tilde{\mathbf{V}}_{j,:})$  is the  $(2r - 2)$ -dimensional manifold:*

$$\mathcal{H}(\tilde{\mathbf{V}}_{j,:}) = \left\{ \phi \in \mathcal{H}_r : \tilde{\mathbf{V}}_{j,:}\tilde{\mathbf{c}}(\phi) = 0 \right\}. \quad (49)$$

**Lemma C.12** (Common Intersection of Group Hypersurfaces). *For any coordinate  $i \in [n]$ , all  $B_K$  hypersurfaces corresponding to the rows of  $\mathcal{G}^{(i)}$  intersect at a common  $(2r - 3)$ -dimensional manifold within  $\mathcal{H}_r$ .*

*Proof.* Let the rows of  $\mathcal{G}^{(i)}$  correspond to row indices  $j_0 = i, j_1 = i + n, \dots, j_{B_K-1} = i + (B_K - 1)n$  in  $\tilde{\mathbf{V}}$ . By construction, row  $j_m$  of  $\tilde{\mathbf{V}}$  is derived from  $\rho_m \mathbf{V}_{i,:}$ . Specifically:

$$\tilde{\mathbf{V}}_{j_m,:} = [\Re\{\rho_m \mathbf{V}_{i,:}\} \quad \Im\{\rho_m \mathbf{V}_{i,:}\}]. \quad (50)$$

The boundary condition  $\tilde{\mathbf{V}}_{j_m,:} \tilde{\mathbf{c}}(\phi) = 0$  is equivalent to:

$$\Im\{\rho_m \mathbf{V}_{i,:} \mathbf{c}(\phi)\} = 0 \quad \Leftrightarrow \quad \Im\{e^{-i\vartheta_m} \alpha_i(\phi)\} = 0, \quad (51)$$

where  $\alpha_i(\phi) := \mathbf{V}_{i,:} \mathbf{c}(\phi) \in \mathbb{C}$ . The condition  $\Im\{e^{-i\vartheta_m} \alpha_i\} = 0$  means that  $\arg(\alpha_i) = \vartheta_m$  or  $\arg(\alpha_i) = \vartheta_m + \pi$ . In other words,  $\alpha_i$  lies on the line through the origin at angle  $\vartheta_m$ .

The intersection of all  $B_K$  hypersurfaces from group  $\mathcal{G}^{(i)}$  is the set of  $\phi$  such that  $\alpha_i(\phi)$  lies on *all* lines at angles  $\vartheta_0, \vartheta_1, \dots, \vartheta_{B_K-1}$  simultaneously. Since these lines all pass through the origin, their common intersection is precisely the origin. Thus:

$$\bigcap_{m=0}^{B_K-1} \mathcal{H}(\tilde{\mathbf{V}}_{j_m,:}) = \{\phi \in \mathcal{H}_r : \alpha_i(\phi) = 0\} = \{\phi \in \mathcal{H}_r : \mathbf{V}_{i,:} \mathbf{c}(\phi) = 0\}. \quad (52)$$

The constraint  $\mathbf{V}_{i,:} \mathbf{c}(\phi) = 0$  is a single complex equation, equivalent to two real equations. Applied to the  $(2r - 1)$ -dimensional hypercube  $\mathcal{H}_r$ , this generically defines a  $(2r - 1 - 2) = (2r - 3)$ -dimensional manifold. □

**Corollary C.13** (Corollary 1 for General  $K$ ). *For any  $K \geq 2$  (even or odd), all  $B_K$  hypersurfaces originating from the same coordinate  $i$  share a common  $(2r - 3)$ -dimensional intersection manifold, namely the locus where  $\mathbf{V}_{i,:} \mathbf{c}(\phi) = 0$ .*

**Remark 11.** *For  $r = 1$ , the common intersection is  $(2 \cdot 1 - 3) = (-1)$ -dimensional, meaning it is generically empty within  $\mathcal{H}_1 = (-\pi/K, \pi/K]$ . This is consistent with the rank-1 algorithm, where each coordinate's boundary points are isolated values  $\varphi_i \in (-\pi/K, \pi/K]$ .*

**Remark 12.** *For  $r = 2$ , the common intersection is  $(2 \cdot 2 - 3) = 1$ -dimensional, i.e., a curve within the 3-dimensional hypercube  $\mathcal{H}_2$ . This is illustrated in Figure 1 of the main text.*

## C.5 Phase Reduction and Equivalent Candidate Elimination

We establish that restricting the final auxiliary angle to  $(-\pi/K, \pi/K]$  is valid for all  $K \geq 2$  and does not lose any optimal solutions.

**Lemma C.14** (Phase Equivalence). *For any  $\mathbf{z} \in \mathcal{A}_K^q$  and any  $\theta \in \mathcal{A}_K$ , we have:*

$$\|\mathbf{V}^\dagger \mathbf{z}\|_2 = \|\mathbf{V}^\dagger(\theta \mathbf{z})\|_2. \quad (53)$$

Consequently, if  $\mathbf{z}^*$  maximizes (24), then so does  $\theta \mathbf{z}^*$  for any  $\theta \in \mathcal{A}_K$ .

*Proof.* We have  $\|\mathbf{V}^\dagger(\theta \mathbf{z})\|_2 = |\theta| \cdot \|\mathbf{V}^\dagger \mathbf{z}\|_2 = \|\mathbf{V}^\dagger \mathbf{z}\|_2$  since  $|\theta| = 1$  for  $\theta \in \mathcal{A}_K$ . □

**Lemma C.15** (Auxiliary Angle Reduction). *Let  $\phi \in \mathcal{H}_r$  with  $\phi_{2r-1} \in (-\pi/K, \pi/K]$ . For any  $k \in \{1, \dots, K - 1\}$ , define  $\phi^{(k)}$  by:*

$$\phi_j^{(k)} = \begin{cases} \phi_j & j \neq 2r - 1, \\ \phi_{2r-1} + \frac{2\pi k}{K} & j = 2r - 1. \end{cases} \quad (54)$$

Then:

$$\mathbf{d}(\mathbf{V}; \phi^{(k)}) = e^{-\frac{2\pi i k}{K}} \mathbf{d}(\mathbf{V}; \phi), \quad (55)$$

where  $\mathbf{d}(\mathbf{V}; \boldsymbol{\phi})$  is the decision function mapping  $\boldsymbol{\phi}$  to the optimal assignment vector.

*Proof.* The complex steering vector satisfies:

$$\mathbf{c}(\boldsymbol{\phi}^{(k)}) = e^{\frac{2\pi ik}{K}} \mathbf{c}(\boldsymbol{\phi}), \quad (56)$$

since the phase shift in  $\phi_{2r-1}$  propagates to the complex exponential in the last component of  $\mathbf{c}$ .

For coordinate  $i$ , the decision rule selects:

$$d_i(\mathbf{V}; \boldsymbol{\phi}^{(k)}) = \arg \max_{z \in \mathcal{A}_K} \Re\{z^* \mathbf{V}_{i,:} \mathbf{c}(\boldsymbol{\phi}^{(k)})\} = \arg \max_{z \in \mathcal{A}_K} \Re\{z^* e^{\frac{2\pi ik}{K}} \mathbf{V}_{i,:} \mathbf{c}(\boldsymbol{\phi})\}. \quad (57)$$

Substituting  $z' = ze^{\frac{2\pi ik}{K}}$ , which is a bijection on  $\mathcal{A}_K$ :

$$d_i(\mathbf{V}; \boldsymbol{\phi}^{(k)}) = e^{-\frac{2\pi ik}{K}} \arg \max_{z' \in \mathcal{A}_K} \Re\{z'^* \mathbf{V}_{i,:} \mathbf{c}(\boldsymbol{\phi})\} = e^{-\frac{2\pi ik}{K}} d_i(\mathbf{V}; \boldsymbol{\phi}). \quad (58)$$

□

□

**Corollary C.16** (No Loss from Restriction). *Restricting  $\phi_{2r-1}$  to  $(-\pi/K, \pi/K]$  instead of  $(-\pi, \pi]$  does not exclude any essentially distinct candidate solutions. Candidate vectors from the unrestricted range are phase rotations of those from the restricted range.*

*Proof.* Any  $\boldsymbol{\phi}$  with  $\phi_{2r-1} \in (-\pi, \pi]$  can be written as  $\boldsymbol{\phi}^{(k)}$  for some  $k \in \{0, \dots, K-1\}$  and some base  $\boldsymbol{\phi}$  with  $\phi_{2r-1} \in (-\pi/K, \pi/K]$ . By Lemmas C.14 and C.15, the candidate from  $\boldsymbol{\phi}^{(k)}$  achieves the same objective value as the candidate from  $\boldsymbol{\phi}$ . □ □

**Proposition C.17** (No Redundant Candidates). *The candidate set  $\mathcal{S}(\mathbf{V})$  constructed from  $\boldsymbol{\phi} \in \mathcal{H}_r$  contains no two candidates that are phase rotations of each other.*

*Proof.* Suppose  $\mathbf{z}, \mathbf{z}' \in \mathcal{S}(\mathbf{V})$  with  $\mathbf{z}' = \theta \mathbf{z}$  for some  $\theta \in \mathcal{A}_K \setminus \{1\}$ . By construction,  $\mathbf{z} = \mathbf{d}(\mathbf{V}; \boldsymbol{\phi})$  and  $\mathbf{z}' = \mathbf{d}(\mathbf{V}; \boldsymbol{\phi}')$  for some  $\boldsymbol{\phi}, \boldsymbol{\phi}' \in \mathcal{H}_r$ .

By Lemma C.15, if  $\mathbf{z}' = e^{-2\pi ik/K} \mathbf{z}$ , then  $\boldsymbol{\phi}'$  must satisfy  $\phi'_{2r-1} = \phi_{2r-1} + 2\pi k/K$ . But for  $k \neq 0$ , this places  $\phi'_{2r-1}$  outside  $(-\pi/K, \pi/K]$ , contradicting  $\boldsymbol{\phi}' \in \mathcal{H}_r$ . □ □

## C.6 Candidate Set Enumeration

We now derive the exact size of the candidate set for general  $K$ .

**Definition C.18** (Vertex of the Arrangement). *A vertex of the hypersurface arrangement is a point  $\boldsymbol{\phi} \in \mathcal{H}_r$  that lies on exactly  $2r - 1$  hypersurfaces from distinct rows of  $\tilde{\mathbf{V}}$ . Formally, for an index set  $\mathcal{I} = \{j_1, \dots, j_{2r-1}\} \subset [B_K n]$  with  $|\mathcal{I}| = 2r - 1$ , the vertex  $\boldsymbol{\phi}(\mathbf{V}; \mathcal{I})$  is the solution (if unique) to:*

$$\tilde{\mathbf{V}}_{\mathcal{I},:} \tilde{\mathbf{c}}(\boldsymbol{\phi}) = \mathbf{0}_{2r-1}. \quad (59)$$

**Lemma C.19** (Vertex Existence and Uniqueness). *For an index set  $\mathcal{I} \subset [B_K n]$  with  $|\mathcal{I}| = 2r - 1$ :*

- (i) *If  $\text{rank}(\tilde{\mathbf{V}}_{\mathcal{I},:}) = 2r - 1$ , there exists a unique  $\tilde{\mathbf{c}} \in \mathbb{R}^{2r}$  (up to scaling) satisfying  $\tilde{\mathbf{V}}_{\mathcal{I},:} \tilde{\mathbf{c}} = \mathbf{0}$ . Converting to hyperpolar coordinates gives at most one  $\boldsymbol{\phi}(\mathbf{V}; \mathcal{I}) \in \mathcal{H}_r$ .*
- (ii) *If  $\text{rank}(\tilde{\mathbf{V}}_{\mathcal{I},:}) < 2r - 1$ , the system has infinitely many solutions, and no unique vertex exists.*

*Proof.* The matrix  $\tilde{\mathbf{V}}_{\mathcal{I},:} \in \mathbb{R}^{(2r-1) \times 2r}$  has nullity at least 1. If rank equals  $2r - 1$ , the null space is one-dimensional, spanned by some  $\tilde{\mathbf{c}}^* \neq \mathbf{0}$ . The hyperpolar parameterization maps each unit vector in  $\mathbb{R}^{2r}$  to a unique  $\boldsymbol{\phi}$ ; normalizing  $\tilde{\mathbf{c}}^*$  gives the vertex coordinates.

If rank is less than  $2r - 1$ , the null space has dimension greater than 1, corresponding to a higher-dimensional manifold of solutions rather than a unique vertex. □ □

**Lemma C.20** (Rank Deficiency from Same-Row Triples). *If  $\mathcal{I}$  contains three or more indices from the same coordinate group  $\mathcal{G}^{(i)}$ , then  $\text{rank}(\tilde{\mathbf{V}}_{\mathcal{I},:}) < 2r - 1$ .*

*Proof.* By Lemma C.12, the hypersurfaces from the same group intersect along a  $(2r-3)$ -manifold. If three or more rows from  $\mathcal{G}^{(i)}$  are in  $\mathcal{I}$ , these rows are linearly dependent when restricted to directions perpendicular to the common intersection manifold. Specifically, if rows  $j_1, j_2, j_3$  all come from group  $\mathcal{G}^{(i)}$ , the system  $\tilde{\mathbf{V}}_{\{j_1, j_2, j_3\},:} \tilde{\mathbf{c}} = \mathbf{0}$  is equivalent to the single complex equation  $\mathbf{V}_{i,:} \mathbf{c} = 0$ , which is only two real equations, not three. Thus the three rows contribute only rank 2, creating rank deficiency.  $\square$   $\square$

**Remark 13** (Rank Structure of Coordinate Groups). *Each coordinate group  $\mathcal{G}^{(i)}$  spans a 2-dimensional subspace of  $\mathbb{R}^{2r}$ . Specifically, all  $B_K$  rows of  $\mathcal{G}^{(i)}$  lie in  $\text{span}\{\tilde{\mathbf{a}}_i, \tilde{\mathbf{b}}_i\}$ , where  $\tilde{\mathbf{a}}_i$  and  $\tilde{\mathbf{b}}_i$  are derived from the real and imaginary parts of  $\mathbf{V}_{i,:}$ . Under the generic assumption that the subspaces corresponding to distinct coordinates are in general position, selecting  $n_i$  rows from group  $\mathcal{G}^{(i)}$  contributes  $\min(n_i, 2)$  to the total rank. Consequently, for an index set  $\mathcal{I}$  with  $n_i$  rows from each group  $i$ , we have*

$$\text{rank}(\tilde{\mathbf{V}}_{\mathcal{I},:}) = \sum_{i:n_i>0} \min(n_i, 2). \quad (60)$$

*This formula confirms that the constraint “at most two rows per group” is both necessary and sufficient for achieving full rank  $2r - 1$ .*

**Definition C.21** (Valid Index Set). *An index set  $\mathcal{I} \subset [B_K n]$  with  $|\mathcal{I}| = 2r - 1$  is valid if it contains at most two indices from each coordinate group  $\mathcal{G}^{(i)}$  for all  $i \in [n]$ .*

**Remark 14** (Mixed Configurations). *The validity condition handles all possible distributions of  $2r - 1$  indices across coordinate groups uniformly. For instance, with  $r = 3$  (requiring  $2r - 1 = 5$  indices):*

- *Distribution (2, 2, 1) across three groups yields rank  $\min(2, 2) + \min(2, 2) + \min(1, 2) = 2 + 2 + 1 = 5$  (valid);*
- *Distribution (3, 1, 1) yields rank  $\min(3, 2) + \min(1, 2) + \min(1, 2) = 2 + 1 + 1 = 4 < 5$  (invalid).*

*More generally, any distribution where multiple groups each contribute two indices remains valid, provided no group contributes three or more.*

**Corollary C.22** (Two Boundaries Implies All Boundaries). *If two distinct hypersurfaces from coordinate group  $\mathcal{G}^{(i)}$  both pass through a point  $\phi^* \in \mathcal{H}_r$ , then  $\mathbf{V}_{i,:} \mathbf{c}(\phi^*) = 0$ , and consequently all  $B_K$  hypersurfaces from group  $\mathcal{G}^{(i)}$  pass through  $\phi^*$ .*

*Proof.* Let  $z = \mathbf{V}_{i,:} \mathbf{c}(\phi^*) \in \mathbb{C}$ . Two hypersurfaces from  $\mathcal{G}^{(i)}$  passing through  $\phi^*$  means  $\Im\{e^{-i\vartheta_{m_1}} z\} = 0$  and  $\Im\{e^{-i\vartheta_{m_2}} z\} = 0$  for distinct boundary angles  $\vartheta_{m_1} \neq \vartheta_{m_2}$ . Writing  $z = |z|e^{i\alpha}$ , these conditions require  $\sin(\alpha - \vartheta_{m_1}) = 0$  and  $\sin(\alpha - \vartheta_{m_2}) = 0$ .

If  $|z| \neq 0$ , then  $\alpha - \vartheta_{m_1} \in \pi\mathbb{Z}$  and  $\alpha - \vartheta_{m_2} \in \pi\mathbb{Z}$ , implying  $\vartheta_{m_1} - \vartheta_{m_2} \in \pi\mathbb{Z}$ . For boundary angles  $\vartheta_m = \frac{\pi(2m+1)}{K}$  with distinct  $m_1, m_2 \in \mathcal{M}_K$ , we have  $\vartheta_{m_1} - \vartheta_{m_2} = \frac{2\pi(m_1 - m_2)}{K}$ , which lies in  $\pi\mathbb{Z}$  only if  $(m_1 - m_2) \in \frac{K}{2}\mathbb{Z}$ . For  $K$  odd this is impossible for distinct indices in  $\mathcal{M}_K = \{0, \dots, K - 1\}$ ; for  $K$  even with  $\mathcal{M}_K = \{0, \dots, K/2 - 1\}$ , the difference  $|m_1 - m_2| < K/2$  also precludes this.

Therefore  $|z| = 0$ , i.e.,  $\mathbf{V}_{i,:} \mathbf{c}(\phi^*) = 0$ . By Lemma C.12, this is precisely the condition for all  $B_K$  hypersurfaces from  $\mathcal{G}^{(i)}$  to pass through  $\phi^*$ .  $\square$   $\square$

**Lemma C.23** (Cells Adjacent to a Vertex). *Let  $\mathcal{I}$  be a valid index set defining a vertex  $\phi(\mathbf{V}; \mathcal{I}) \in \mathcal{H}_r$ . Let  $p$  denote the number of coordinate groups that contribute exactly two indices to  $\mathcal{I}$ . Then the vertex is adjacent to exactly  $(B_K - 1)^p$  cells in the hypersurface arrangement.*

*Proof.* Let  $\mathcal{I}$  be a valid index set with  $p$  coordinate groups each contributing exactly two indices. By Corollary C.22, for each such group  $\mathcal{G}^{(i)}$ , all  $B_K$  hypersurfaces pass through the vertex  $\phi^* = \phi(\mathbf{V}; \mathcal{I})$ .

Consider the local geometry at  $\phi^*$ . For a coordinate group  $\mathcal{G}^{(i)}$  contributing two indices to  $\mathcal{I}$ :

- All  $B_K$  hypersurfaces from  $\mathcal{G}^{(i)}$  pass through  $\phi^*$ ;

- These hypersurfaces share a common  $(2r - 3)$ -dimensional intersection (where  $\mathbf{V}_{i,:}\mathbf{c}(\phi) = 0$ );
- In the 2-dimensional normal space to this intersection, the  $B_K$  hypersurfaces appear as  $B_K$  lines through the origin;
- These  $B_K$  lines divide the 2D normal space into  $2B_K$  angular sectors;
- However, antipodal sectors correspond to the same symbol assignment (since  $\Re\{z^*\alpha_i\}$  has the same sign for  $\alpha_i$  and  $-\alpha_i$  when  $z$  is fixed);
- Thus there are  $B_K$  distinct symbol regions for coordinate  $i$ .

For a coordinate contributing exactly one index to  $\mathcal{I}$ , only that single hypersurface generically passes through  $\phi^*$ , dividing a neighborhood into 2 half-spaces with distinct symbol assignments.

The  $2r - 1$  defining constraints come from  $p$  groups contributing 2 each (total  $2p$  constraints, but only  $2p$  dimensions of freedom due to the 2D subspace structure) and  $(2r - 1 - 2p)$  groups contributing 1 each. At the vertex:

- Each of the  $p$  saturated groups offers  $B_K$  symbol choices (one per angular sector);
- Each of the  $(2r - 1 - 2p)$  non-saturated groups offers 2 symbol choices (one per half-space).

However, moving away from the vertex into a cell requires consistent choices. The two indices from each saturated group define two of the  $B_K$  hypersurfaces; moving into a cell means choosing one of the  $B_K - 1$  “wedges” between consecutive hypersurfaces that does not cross either defining hypersurface immediately. This gives  $(B_K - 1)$  choices per saturated group.

For non-saturated groups, the single defining hypersurface is crossed or not, but since we are counting cells (not half-cells), each non-saturated group contributes a factor of 1 to the cell count (the symbol is determined by which side of the hypersurface the cell lies on).

Therefore, the number of cells adjacent to the vertex is  $(B_K - 1)^p$ .  $\square$

**Theorem 15** (Candidate Set Size for General  $K$ ). *For a rank- $r$  matrix with factor  $\mathbf{V} \in \mathbb{C}^{n \times r}$  and alphabet  $\mathcal{A}_K$  with effective boundary count  $B_K$ , the candidate set satisfies:*

$$|\mathcal{S}(\mathbf{V})| = \sum_{d=1}^r \sum_{i=0}^{d-1} \binom{n}{i} \binom{n-i}{2(d-i)-1} B_K^{2(d-i)-2} (B_K - 1)^i. \quad (61)$$

For fixed  $K$  and  $r$ , this is  $O(n^{2r-1})$ .

*Proof.* We count candidates at each rank level  $d = 1, \dots, r$  and sum.

**Counting at rank  $d$ :** Consider valid index sets  $\mathcal{I} \subset [B_K n]$  with  $|\mathcal{I}| = 2d - 1$  that define vertices in the interior of  $\mathcal{H}_d$  (the rank- $d$  hypercube). Let  $i$  denote the number of coordinate groups contributing exactly two indices to  $\mathcal{I}$ .

*Step 1: Choose which coordinates contribute two indices.* There are  $\binom{n}{i}$  ways to select  $i$  coordinates from  $[n]$ .

*Step 2: Choose which two boundaries from each such coordinate.* For each of the  $i$  coordinates, we select 2 boundaries from  $B_K$  options. There are  $\binom{B_K}{2}$  ways per coordinate, giving  $\binom{B_K}{2}^i$  total.

*Step 3: Choose remaining coordinates contributing one index each.* The remaining  $2d - 1 - 2i$  indices come from  $2d - 1 - 2i$  distinct coordinates (other than the  $i$  already chosen). There are  $\binom{n-i}{2d-1-2i}$  ways to select these coordinates.

*Step 4: Choose which boundary from each single-index coordinate.* For each of the  $2d - 1 - 2i$  coordinates, we select 1 boundary from  $B_K$  options, giving  $B_K^{2d-1-2i}$  combinations.

*Step 5: Count cells per vertex.* By Lemma C.23, each such vertex is adjacent to  $(B_K - 1)^i$  cells.

Combining:

$$|\mathcal{J}(\mathbf{V}_{:,1:d})| = \sum_{i=0}^{d-1} \binom{n}{i} \binom{B_K}{2}^i \binom{n-i}{2d-1-2i} B_K^{2d-1-2i} (B_K - 1)^i. \quad (62)$$

The total candidate set size is:

$$|\mathcal{S}(\mathbf{V})| = \sum_{d=1}^r |\mathcal{J}(\mathbf{V}_{:,1:d})| = \sum_{d=1}^r \sum_{i=0}^{d-1} \binom{n}{i} \binom{n-i}{2(d-i)-1} B_K^{2(d-i)-2} (B_K - 1)^i, \quad (63)$$

where the sum over  $d$  accounts for the recursive structure handling boundary cases.

**Asymptotic analysis:** For fixed  $K$  and  $d$ , the dominant term is  $i = 0$ :

$$\binom{n}{2d-1} B_K^{2d-2} = O(n^{2d-1}). \quad (64)$$

Summing over  $d = 1, \dots, r$ :  $|\mathcal{S}(\mathbf{V})| = O(rn^{2r-1})$ . □ □

## C.7 Algorithm Correctness for General $K$

We now prove that Algorithm 2 (with the augmented matrix constructed for general  $K$  as in Section C.3) correctly solves the discrete quadratic maximization problem.

**Theorem 16** (Correctness for General  $K$ ). *Let  $\mathbf{Q} = \mathbf{V}\mathbf{V}^\dagger \in \mathbb{C}^{n \times n}$  be a rank- $r$  PSD matrix and let  $K \geq 2$  be arbitrary. Algorithm 2, using the augmented matrix  $\tilde{\mathbf{V}} \in \mathbb{R}^{B_K n \times 2r}$  constructed as in Definition C.8, returns  $\mathbf{z}^* \in \mathcal{A}_K^n$  satisfying:*

$$\mathbf{z}^{*\dagger} \mathbf{Q} \mathbf{z}^* = \max_{\mathbf{z} \in \mathcal{A}_K^n} \mathbf{z}^\dagger \mathbf{Q} \mathbf{z}. \quad (65)$$

*Proof.* We show that the candidate set  $\mathcal{S}(\mathbf{V})$  enumerated by the algorithm contains the global maximizer.

**Step 1: Reformulation as double maximization.** By the Cauchy-Schwarz argument (Lemma C.1 and the subsequent discussion):

$$\max_{\mathbf{z} \in \mathcal{A}_K^n} \|\mathbf{V}^\dagger \mathbf{z}\|_2 = \max_{\phi \in \mathcal{H}_r} \max_{\mathbf{z} \in \mathcal{A}_K^n} \Re\{\mathbf{z}^\dagger \mathbf{V} \mathbf{c}(\phi)\} = \max_{\phi \in \mathcal{H}_r} \sum_{i=1}^n \max_{z_i \in \mathcal{A}_K} \Re\{z_i^* \mathbf{V}_{i,:} \mathbf{c}(\phi)\}. \quad (66)$$

The second equality holds because, for fixed  $\phi$ , the coordinates  $z_i$  can be optimized independently.

**Step 2: Decision function is piecewise constant.** For fixed  $\phi$ , the optimal  $z_i$  is determined by the decision rule:

$$d_i(\mathbf{V}; \phi) = \arg \max_{z \in \mathcal{A}_K} \Re\{z^* \mathbf{V}_{i,:} \mathbf{c}(\phi)\}. \quad (67)$$

Let  $\alpha_i(\phi) = \mathbf{V}_{i,:} \mathbf{c}(\phi)$ . The optimal  $z_i$  is the element of  $\mathcal{A}_K$  whose phase is closest to  $\arg(\alpha_i(\phi))$ . As  $\phi$  varies, the phase of  $\alpha_i$  varies continuously, and  $d_i$  changes only when  $\arg(\alpha_i)$  crosses a boundary angle  $\vartheta_m$ .

**Step 3: Hypersurfaces partition  $\mathcal{H}_r$  into cells.** The  $B_K n$  hypersurfaces  $\{\mathcal{H}(\tilde{\mathbf{V}}_{j,:})\}_{j=1}^{B_K n}$  partition  $\mathcal{H}_r$  into cells. Within each cell, the decision function  $\mathbf{d}(\mathbf{V}; \phi)$  is constant. The objective  $\sum_i \max_{z_i} \Re\{z_i^* \alpha_i(\phi)\}$  is continuous in  $\phi$ , so the global maximum is attained either:

- (a) At a vertex of the arrangement (intersection of  $2r - 1$  hypersurfaces), or
- (b) On the boundary of  $\mathcal{H}_r$ .

**Step 4: Enumeration of interior vertices.** The main loop of Algorithm 2 enumerates all valid index sets  $\mathcal{I} \subset [B_K n]$  with  $|\mathcal{I}| = 2r - 1$  and checks if  $\text{rank}(\tilde{\mathbf{V}}_{\mathcal{I},:}) = 2r - 1$ . For each such  $\mathcal{I}$ , it computes the vertex  $\phi(\mathbf{V}; \mathcal{I})$ , applies the decision rule to obtain a candidate  $\mathbf{z}_{\mathcal{I}}$ , and evaluates the objective.

By Lemma C.19, this enumeration covers all cells whose "leading vertex" (the vertex with minimal  $\phi_{2r-1}$ ) lies in the interior of  $\mathcal{H}_r$ .

**Step 5: Recursive handling of boundary cases.** Cells touching the boundary  $\phi_{2r-1} = -\pi/K$  or  $\phi_{2r-1} = \pi/K$  are not captured by interior vertices. However:

- By Corollary C.16, candidates from  $\phi_{2r-1} = -\pi/K$  are phase rotations of candidates from elsewhere, so no loss occurs.

- Candidates from  $\phi_{2r-2} = \pm\pi/2$  (with arbitrary  $\phi_{2r-1}$ ) correspond to the rank- $(r-1)$  problem on  $\mathbf{V}_{:,1:r-1}$ . The recursive call handles these.

Overall, the boundary of the hypercube  $\mathcal{H}_r$  consists of faces where one angular coordinate is fixed at its extreme value. When this occurs, one degree of freedom in the auxiliary vector  $\mathbf{c}(\phi)$  is eliminated: either a magnitude allocation coordinate ( $\phi_j = \pm\pi/2$ ) becomes extremal, or the final phase coordinate ( $\phi_{2r-1} = \pm\pi/K$ ) is fixed. In both cases, the effective optimization over the remaining  $2(r-1) - 1$  free parameters reduces to a rank- $(r-1)$  subproblem, which is solved by the recursive call in Algorithm 2. This is proven in [KK14].

This reduction is independent of the alphabet size  $K$ . The specific boundary values differ with  $K$  (e.g.,  $\pm\pi/K$  for the phase coordinate), but the mechanism (fixing one coordinate eliminates one degree of freedom) is purely structural. Combined with the interior vertex enumeration, this ensures that the candidate set contains the global optimizer for any rank- $r$  PSD matrix and any  $K \geq 2$ .

**Step 6: Completeness of candidate set.** Combining Steps 4 and 5, every cell of the arrangement is associated with at least one candidate in  $\mathcal{S}(\mathbf{V})$ . Since the global maximizer lies in some cell, it is in  $\mathcal{S}(\mathbf{V})$ .

**Step 7: Evaluation and selection.** The algorithm evaluates the objective for all candidates and returns the best one. Since the global maximizer is in  $\mathcal{S}(\mathbf{V})$ , the returned  $\mathbf{z}^*$  achieves the maximum.  $\square$   $\square$

**Corollary C.24** (Correctness for  $K = 3$ ). *For  $K = 3$ , Algorithm 2 with  $\tilde{\mathbf{V}} \in \mathbb{R}^{3n \times 2r}$  exactly solves the Max-3-Cut problem formulated as (2).*

*Proof.* Immediate from Theorem 16 with  $K = 3$ , noting that for  $K = 3$  the complex quadratic form corresponds to the Max-3-Cut objective.  $\square$

## C.8 Comparison: Even vs. Odd $K$

We summarize the key differences between even and odd  $K$  in Table 2.

Table 2: Comparison of algorithm structure for even and odd  $K$ .

Aspect	Even $K$ [KL06]	Odd $K$
Antipodal symmetry	Present ( $-1 \in \mathcal{A}_K$ )	Absent
Boundaries per coordinate ( $B_K$ )	$K/2$	$K$
Augmented matrix rows	$nK/2$	$nK$
Rotation factors	$\{e^{-i\pi(2m+1)/K}\}_{m=0}^{K/2-1}$	$\{e^{-i\pi(2m+1)/K}\}_{m=0}^{K-1}$
Group intersection property	All $K/2$ hypersurfaces share axis	All $K$ hypersurfaces share axis
Cells adjacent to vertex	$(K/2 - 1)^p$	$(K - 1)^p$
Index sets to enumerate	$O((nK/2)^{2r-1})$	$O((nK)^{2r-1})$
Valid index sets	$O(n^{2r-1})$	$O(n^{2r-1})$
Candidate set size	Formula with $B_K = K/2$	Formula with $B_K = K$

## D Additional Theoretical Guarantees and Proofs on Perturbed Low-Rank Matrices

### D.1 Useful Facts

In these proofs, we are going to use the following theorems.

**Theorem 17** (Wedin's Theorem [Wed72]). Let  $\mathbf{M}, \widetilde{\mathbf{M}} \in \mathbb{C}^{m \times n}$  be two matrices with rank- $r$  SVDs:

$$\begin{aligned}\mathbf{M} &= [\mathbf{U}_1 \quad \mathbf{U}_2] \begin{bmatrix} \boldsymbol{\Sigma}_1 & 0 \\ 0 & \boldsymbol{\Sigma}_2 \end{bmatrix} \begin{bmatrix} \mathbf{V}_1^\top \\ \mathbf{V}_2^\top \end{bmatrix}; \\ \widetilde{\mathbf{M}} = \mathbf{M} + \boldsymbol{\Delta} &= [\widetilde{\mathbf{U}}_1 \quad \widetilde{\mathbf{U}}_2] \begin{bmatrix} \widetilde{\boldsymbol{\Sigma}}_1 & 0 \\ 0 & \widetilde{\boldsymbol{\Sigma}}_2 \end{bmatrix} \begin{bmatrix} \widetilde{\mathbf{V}}_1^\top \\ \widetilde{\mathbf{V}}_2^\top \end{bmatrix}.\end{aligned}$$

Let  $\sigma_j, \widetilde{\sigma}_j$  denote the  $j$ th singular value of  $\mathbf{M}, \widetilde{\mathbf{M}}$ , respectively, and let  $\boldsymbol{\Delta} = \mathbf{M} - \widetilde{\mathbf{M}}$ . If  $\delta = \min \{ \min_{1 \leq i \leq r, r+1 \leq j \leq n} |\sigma_i - \widetilde{\sigma}_j|, \min_{1 \leq i \leq r} \sigma_i \} > 0$ , then:

$$\begin{aligned}\max \left\{ \left\| (\mathbf{I} - \mathbf{U}_1 \mathbf{U}_1^\top) \widetilde{\mathbf{U}}_1 \right\|_2, \left\| (\mathbf{I} - \mathbf{V}_1 \mathbf{V}_1^\top) \widetilde{\mathbf{V}}_1 \right\|_2 \right\} \\ \leq \frac{\|\boldsymbol{\Delta}\|_2}{\delta}\end{aligned}$$

**Theorem 18** (Proposition 3.1 of [BAL19]). Let  $\mathbf{M} \in \mathbb{C}^{n \times n}$  be a square matrix with independently entries  $\mathbf{M}_{ij} \in \text{subG}(1)$ . Then there exists constant  $C, c > 0$  such that for all  $A \geq C$ , with probability at least  $1 - C \exp(-cAn)$ , we have that  $\|\mathbf{M}\|_2 \leq A\sqrt{n}$ .

## D.2 Proof of Theorem 4

**Theorem 4.** Let  $\mathbf{z}_r, \text{OPT-}\mathbf{Q}^*$  be defined in (17). Let  $\lambda_j^*$  be the  $j$ th eigenvalue of  $\mathbf{Q}^*$  with  $\lambda_j^* = 0$  if  $j > r$ , and define the eigengap of  $\mathbf{Q}$  as  $\delta^* = \min \{ \min_{j \in [r-1]} |\lambda_j^* - \lambda_{j+1}^*|, \lambda_r^* \}$ . If  $r \leq r^*$  and  $\|\mathbf{H}\|_2 \leq \frac{\delta^*}{2}$ , then we have that:

$$|\text{OPT-}\mathbf{Q}^* - \mathbf{z}_r^\dagger \mathbf{Q}^* \mathbf{z}_r| \leq O \left( n \left( \lambda_{r+1}^* + \frac{\lambda_1^*}{\delta^*} \|\mathbf{H}\|_2 \right) \right). \quad (18)$$

Recall the following definitions:

- $\mathbf{Q}^* \in \mathbb{C}^{n \times n}$  is Hermitian PSD with eigendecomposition  $\mathbf{Q}^* = \sum_{i=1}^{r^*} \lambda_i^* \mathbf{u}_i^* \mathbf{u}_i^{*\dagger}$
- $\mathbf{Q} = \mathbf{Q}^* + \mathbf{H}$  with SVD  $\mathbf{Q} = \sum_{i=1}^n \lambda_i \mathbf{u}_i \mathbf{v}_i^\dagger$
- $\mathbf{Q}_r = \sum_{i=1}^r \lambda_i \mathbf{u}_i \mathbf{u}_i^\dagger$
- $\mathbf{z}^*$  attains  $\text{OPT-}\mathbf{Q}^* = \max_{\mathbf{z} \in \mathcal{A}_K^n} \mathbf{z}^\dagger \mathbf{Q}^* \mathbf{z}$
- $\mathbf{z}_r := \arg \max_{\mathbf{z} \in \mathcal{A}_K^n} \mathbf{z}^\dagger \mathbf{Q}_r \mathbf{z}$

We require the following general lemma to prove the theorems of interest.

**Lemma D.1.** Let  $\mathbf{Q}^*, \mathbf{Q}_r, \mathbf{z}^*$ , and  $\mathbf{z}_r$  be defined above. Then we have that

$$|\mathbf{z}^{*\dagger} \mathbf{Q}^* \mathbf{z}^* - \mathbf{z}_r^\dagger \mathbf{Q}^* \mathbf{z}_r| \leq n \|\mathbf{Q}^* - \mathbf{Q}_r\|_2$$

*Proof.* Since for all  $\mathbf{z} \in \mathcal{A}_K^n$  we have that  $|\mathbf{z}| = 1$ , we must have that  $\|\mathbf{z}\|_2^2 = n$  for all  $\mathbf{z} \in \mathcal{A}_K^n$ . We decompose

the quantity of interest as

$$\begin{aligned}
& \left| \mathbf{z}^{\star\dagger} \mathbf{Q}^* \mathbf{z}^* - \mathbf{z}_r \mathbf{Q}^* \mathbf{z}_r \right| \\
&= \left| \mathbf{z}^{\star\dagger} \mathbf{Q}^* \mathbf{z}^* - \mathbf{z}_r \widehat{\mathbf{Q}} \mathbf{z}_r + \mathbf{z}_r \widehat{\mathbf{Q}} \mathbf{z}_r - \mathbf{z}_r \mathbf{Q}^* \mathbf{z}_r \right| \\
&\leq \left| \mathbf{z}^{\star\dagger} \mathbf{Q}^* \mathbf{z}^* - \mathbf{z}_r \widehat{\mathbf{Q}} \mathbf{z}_r \right| + \left| \mathbf{z}_r \widehat{\mathbf{Q}} \mathbf{z}_r - \mathbf{z}_r \mathbf{Q}^* \mathbf{z}_r \right| \\
&= \left| \max_{\mathbf{z} \in \mathcal{A}_K^n} \mathbf{z}^\dagger \mathbf{Q}^* \mathbf{z} - \max_{\mathbf{z} \in \mathcal{A}_K^n} \mathbf{z}^\dagger \widehat{\mathbf{Q}} \mathbf{z} \right| \\
&\quad + \left| \mathbf{z}_r \widehat{\mathbf{Q}} \mathbf{z}_r - \mathbf{z}_r \mathbf{Q}^* \mathbf{z}_r \right| \\
&\leq \max_{\mathbf{z} \in \mathcal{A}_K^n} \left| \mathbf{z}^\dagger \mathbf{Q}^* \mathbf{z} - \mathbf{z}^\dagger \widehat{\mathbf{Q}} \mathbf{z} \right| + \left| \mathbf{z}_r \widehat{\mathbf{Q}} \mathbf{z}_r - \mathbf{z}_r \mathbf{Q}^* \mathbf{z}_r \right| \\
&\leq \left\| \mathbf{Q}^* - \widehat{\mathbf{Q}} \right\|_2 \cdot \max_{\mathbf{z} \in \mathcal{A}_K^n} \|\mathbf{z}\|_2^2 + \left\| \mathbf{Q}^* - \widehat{\mathbf{Q}} \right\|_2 \|\mathbf{z}_r\|_2^2 \\
&\leq 2n \left\| \mathbf{Q}^* - \widehat{\mathbf{Q}} \right\|_2
\end{aligned}$$

where the last inequality follows from the fact that  $\|\mathbf{z}\|_2^2 = n$  for all  $\mathbf{z} \in \mathcal{A}_K^n$ .  $\square$

To handle the non-Hermitian noise in Theorem 4, we first prove an auxiliary lemma.

**Lemma D.2.** *Let  $\mathbf{Q}^*, \mathbf{Q}, \mathbf{Q}_r, \mathbf{H} \in \mathbb{C}^{n \times n}$  be defined above. Let  $\lambda_j$  be the  $j$ th eigenvalue of  $\mathbf{Q}^*$ , and define  $\delta^* = \min \{ \min_{j \in [r-1]} |\lambda_j^* - \lambda_{j+1}^*|, \lambda_r^* \}$ . If  $\|\mathbf{H}\|_2 \leq \frac{\delta^*}{2}$ , then we have that*

$$\left\| \mathbf{Q}^* - \widehat{\mathbf{Q}} \right\|_2 \leq O \left( \lambda_{r+1}^* + \frac{\lambda_1^*}{\delta^*} \|\mathbf{H}\|_2 \right)$$

*Proof.* Since  $\mathbf{Q}^*$  is Hermitian PSD, we write its top- $r$  eigendecomposition as  $\mathbf{Q}^* = \mathbf{U}^* \mathbf{\Lambda}^* \mathbf{U}^{\star\dagger}$  with  $\mathbf{U}^* \in \mathbb{C}^{n \times r}$  and  $\mathbf{\Lambda}^* \in \mathbb{R}^{r \times r}$  being a diagonal matrix. Let  $\mathbf{u}_j^*$  and  $\mathbf{u}_j$  denote the  $j$ th column of  $\mathbf{U}^*$  and  $\mathbf{U}$ , respectively. Thus, we can decompose the quantity of interest as

$$\begin{aligned}
\left\| \mathbf{Q}^* - \widehat{\mathbf{Q}} \right\|_2 &\leq \left\| \mathbf{Q}^* - \mathbf{U}^* \mathbf{\Lambda}^* \mathbf{U}^{\star\dagger} \right\|_2 \\
&\quad + \left\| \mathbf{U}^* \mathbf{\Lambda}^* \mathbf{U}^{\star\dagger} - \mathbf{U} \mathbf{\Lambda}^* \mathbf{U}^\dagger \right\|_2 \\
&\quad + \left\| \mathbf{U} \mathbf{\Lambda}^* \mathbf{U}^\dagger - \widehat{\mathbf{Q}} \right\|_2
\end{aligned} \tag{68}$$

For the first term, since we know that  $\mathbf{U}^* \mathbf{\Lambda}^* \mathbf{U}^{\star\dagger}$  is the top- $r$  truncated SVD of  $\mathbf{Q}^*$ , we can simply bound

$$\left\| \mathbf{Q}^* - \mathbf{U}^* \mathbf{\Lambda}^* \mathbf{U}^{\star\dagger} \right\|_2 \leq \lambda_{r+1}^* \tag{69}$$

For the third term, we have that

$$\begin{aligned}
\left\| \mathbf{U} \mathbf{\Lambda}^* \mathbf{U}^\dagger - \widehat{\mathbf{Q}} \right\|_2 &= \left\| \mathbf{U} (\mathbf{\Lambda}^* - \mathbf{\Sigma}) \mathbf{U}^\dagger \right\|_2 \\
&= \left\| \mathbf{\Lambda}^* - \mathbf{\Sigma} \right\|_2 \\
&= \max_{j \in [r]} |\mathbf{\Lambda}_{jj}^* - \mathbf{\Sigma}_{jj}| \\
&\leq \|\mathbf{H}\|_2
\end{aligned} \tag{70}$$

where the last inequality follows from Weyl's inequality due to the fact that  $\mathbf{\Lambda}_{jj}$  and  $\mathbf{\Sigma}_{jj}$  are the singular

values of  $\mathbf{Q}^*$  and  $\mathbf{Q}$ , respectively. For the second term, we can write

$$\begin{aligned}
& \left\| \mathbf{U}^* \mathbf{\Lambda}^* \mathbf{U}^{*\dagger} - \widehat{\mathbf{Q}} \right\|_2 \\
&= \left\| \mathbf{U}^* \mathbf{\Lambda}^* \mathbf{U}^{*\dagger} - \mathbf{U} \mathbf{\Lambda}^* \mathbf{U}^\dagger \right\|_2 \\
&= \left\| \mathbf{U}^* \mathbf{\Lambda}^* (\mathbf{U}^* - \mathbf{U})^\dagger + (\mathbf{U}^* - \mathbf{U}) \mathbf{\Lambda}^* \mathbf{U}^\dagger \right\|_2 \\
&\leq \left\| \mathbf{U}^* \mathbf{\Lambda}^* (\mathbf{U}^* - \mathbf{U})^\dagger \right\|_2 + \left\| (\mathbf{U}^* - \mathbf{U}) \mathbf{\Lambda}^* \mathbf{U}^\dagger \right\|_2 \\
&\leq 2 \left\| \mathbf{\Lambda}^* (\mathbf{U}^* - \mathbf{U})^\dagger \right\|_2 \\
&\leq 2\lambda_1^* \|\mathbf{U}^* - \mathbf{U}\|_2
\end{aligned} \tag{71}$$

where the second-to-last inequality is because  $\max\{\|\mathbf{U}^*\|_2, \|\mathbf{U}\|_2\} \leq 1$  due to the fact that  $\mathbf{U}^*, \mathbf{U}$  contains orthogonal columns. Next, we will study the term  $\|\mathbf{U}^* - \mathbf{U}\|_2$  using Wedin's Theorem. To start, we notice that

$$\begin{aligned}
\|\mathbf{U}^* - \mathbf{U}\|_2 &= \|\mathbf{U}^* - (\mathbf{I} - \mathbf{U}^* \mathbf{U}^{*\dagger}) \mathbf{U} + \mathbf{U}^* \mathbf{U}^{*\dagger} \mathbf{U}\|_2 \\
&\leq \|(\mathbf{I} - \mathbf{U}^* \mathbf{U}^{*\dagger}) \mathbf{U}\|_2 + \|\mathbf{U}^* (\mathbf{I} - \mathbf{U}^{*\dagger} \mathbf{U})\|_2
\end{aligned}$$

Since  $\mathbf{U}^*$  and  $\mathbf{U}$  are the top- $r$  singular vector of  $\mathbf{Q}^*$  and  $\mathbf{Q}$ , respectively, the first term can be simply bounded by Theorem 17 using

$$\|(\mathbf{I} - \mathbf{U}^* \mathbf{U}^{*\dagger}) \mathbf{U}\|_2 \leq \frac{\|\mathbf{H}\|_2}{\delta}$$

For the second term, we have that

$$\begin{aligned}
\|\mathbf{U}^* (\mathbf{I} - \mathbf{U}^{*\dagger} \mathbf{U})\|_2 &\leq \|\mathbf{I} - \mathbf{U}^{*\dagger} \mathbf{U}\|_2 \\
&= \max_{i \in [r]} |1 - \sigma_r(\mathbf{U}^{*\dagger} \mathbf{U})| \\
&= 1 - \sigma_{\min}(\mathbf{U}^{*\dagger} \mathbf{U})
\end{aligned}$$

where the first inequality is due to the fact that  $\|\mathbf{U}\|_2^*$  is a unitary matrix, and the last inequality is because  $\mathbf{U}^{*\dagger} \mathbf{U}$  has singular values in the range  $[0, 1]$ . Let  $\mathbf{x} \in \mathbb{C}^r$  with  $\|\mathbf{x}\|_2 = 1$  be given such that  $\|\mathbf{U}^{*\dagger} \mathbf{U} \mathbf{x}\|_2 = \sigma_{\min}(\mathbf{U}^{*\dagger} \mathbf{U})$ . Then we must have that  $\|\mathbf{U} \mathbf{x}\|_2 = 1$  since  $\mathbf{U}$  contains orthonormal columns. Then we have that

$$\begin{aligned}
\sigma_{\min}(\mathbf{U}^{*\dagger} \mathbf{U}) &= \|\mathbf{U}^{*\dagger} \mathbf{U} \mathbf{x}\|_2 \\
&= \|\mathbf{U}^* \mathbf{U}^{*\dagger} \mathbf{U} \mathbf{x}\|_2 \\
&= 1 - \|(\mathbf{I} - \mathbf{U}^* \mathbf{U}^{*\dagger}) \mathbf{U} \mathbf{x}\|_2 \\
&\geq 1 - \|(\mathbf{I} - \mathbf{U}^* \mathbf{U}^{*\dagger}) \mathbf{U}\|_2
\end{aligned}$$

Thus, the second term can be upper bounded by

$$\begin{aligned}
\|\mathbf{U}^* (\mathbf{I} - \mathbf{U}^{*\dagger} \mathbf{U})\|_2 &= 1 - \sigma_{\min}(\mathbf{U}^{*\dagger} \mathbf{U}) \\
&\leq \|(\mathbf{I} - \mathbf{U}^* \mathbf{U}^{*\dagger}) \mathbf{U}\|_2 \\
&\leq \frac{\|\mathbf{H}\|_2}{\delta}
\end{aligned}$$

Therefore, we can conclude that  $\|\mathbf{U}^* - \mathbf{U}\|_2 \leq \frac{2}{\delta} \|\mathbf{H}\|_2$ , which leads to

$$\left\| \mathbf{U}^* \mathbf{\Lambda}^* \mathbf{U}^{*\dagger} - \widehat{\mathbf{Q}} \right\|_2 \leq \frac{4\lambda_1^*}{\delta} \|\mathbf{H}\|_2 \tag{72}$$

by (71). Plugging (69), (72) and (70) back into (68) gives

$$\left\| \mathbf{Q}^* - \widehat{\mathbf{Q}} \right\|_2 \leq \lambda_{r+1}^* + \left( 1 + \frac{4\lambda_1^*}{\delta} \right) \|\mathbf{H}\|_2$$

Define  $\delta^* = \min \{ \min_{j \in [r-1]} |\lambda_j^* - \lambda_{j+1}^*|, \lambda_r^* \}$ . By Weyl's inequality, we have that  $|\lambda_i^* - \sigma_i| \leq \|\mathbf{H}\|_2$ . Thus, if  $\|\mathbf{H}\|_2 \leq \frac{\delta^*}{2}$ , we can guarantee that  $\sigma_i \in [\lambda_{i-1}^* + \lambda_i^*/2, \lambda_i^* + \lambda_{i+1}^*/2]$ , which implies that

$$\begin{aligned} & \min_{j \in [r-1]} |\lambda_j^* - \sigma_i| \\ & \geq \min \{ |\lambda_{i-1}^* - \sigma_i|, |\lambda_{i+1}^* - \sigma_i| \} \\ & \geq \min \{ |\lambda_{i-1}^* - \lambda_i^*|, |\lambda_{i+1}^* - \lambda_i^*| \} - \|\mathbf{H}\|_2 \\ & \geq \delta^* - \|\mathbf{H}\|_2 \\ & \geq \frac{\delta^*}{2} \end{aligned}$$

for all  $i \in [r]$ . This gives that  $\delta \geq \frac{\delta^*}{2}$ , which implies that

$$\left\| \mathbf{Q}^* - \widehat{\mathbf{Q}} \right\|_2 \leq \lambda_{r+1}^* + \left( 1 + \frac{8\lambda_1^*}{\delta^*} \right) \|\mathbf{H}\|_2$$

Notice that  $\delta^* \leq \lambda_1$ . Therefore, we must have that  $\frac{\lambda_1^*}{\delta^*} \geq 1$ , which implies that  $1 + \frac{8\lambda_1^*}{\delta^*} \leq O\left(\frac{\lambda_1^*}{\delta^*}\right)$ . This concludes the proof.  $\square$

Now, we are ready to prove Theorem 4.

*Proof of Theorem 4.* Under the provided condition, we can apply Lemma D.2 to obtain that

$$\left\| \mathbf{Q}^* - \widehat{\mathbf{Q}} \right\|_2 \leq O\left( \lambda_{r+1}^* + \frac{\lambda_1^*}{\delta^*} \|\mathbf{H}\|_2 \right)$$

Plugging the bound into Lemma D.1 gives

$$|\mathbf{z}^{*\dagger} \mathbf{Q}^* \mathbf{z}^* - \mathbf{z}_r \mathbf{Q}^* \mathbf{z}_r| \leq O\left( n \left( \lambda_{r+1}^* + \frac{\lambda_1^*}{\delta^*} \|\mathbf{H}\|_2 \right) \right)$$

$\square$

### D.3 Removing the dependence on the eigengap

One should notice that, in Theorem 4, both the requirement  $\|\mathbf{H}\|_2 \leq \frac{\delta^*}{2}$  and the upper bound in depend on the eigengap  $\delta^*$ . Such a dependency appears because we need to explicitly construct the Hermitian matrix  $\mathbf{Q}_r$  from the non-Hermitian  $\mathbf{Q}$ , which naturally introduced the eigenvector perturbation  $\mathbf{u}_i$  from  $\mathbf{u}_i^*$  due to  $\mathbf{H}$ . It is common in prior work that such eigenvector perturbation bound involves a dependency on the eigengap  $\delta^*$  [CCF18, Wed72]. The corollary below shows that we can drop the dependency on the eigengap if the perturbation matrix  $\mathbf{H}$  is Hermitian:

**Corollary D.3.** *Let  $\mathbf{z}_r, OPT\text{-}\mathbf{Q}^*$  be defined in (17). Let  $\lambda_j^*$  be the  $j$ th eigenvalue of  $\mathbf{Q}^*$  with  $\lambda_j^* = 0$  if  $j > r$ . If  $r \leq r^*$  and  $\mathbf{H}$  is Hermitian, then we have that:*

$$|OPT\text{-}\mathbf{Q}^* - \mathbf{z}_r^\dagger \mathbf{Q}^* \mathbf{z}_r| \leq O\left( n \left( \lambda_{r+1}^* + \|\mathbf{H}\|_2 \right) \right). \quad (73)$$

In short, Corollary D.3 saves a multiplicative factor of  $\frac{\lambda_1^*}{\delta^*}$  compared with Theorem 4 by assuming that  $\mathbf{H}$  is Hermitian.

The following lemma provides an upper bound of the approximation error when the perturbation  $\mathbf{H}$  (and consequently  $\mathbf{Q}$ ) is Hermitian

**Lemma D.4.** *Let  $\mathbf{Q}^*, \mathbf{Q}, \mathbf{Q}_r, \mathbf{H} \in \mathbb{C}^{n \times n}$  be defined above. Let  $\lambda_j$  be the  $j$ th eigenvalue of  $\mathbf{Q}^*$ . If  $\mathbf{H}$  is Hermitian, then we have that*

$$\left\| \mathbf{Q}^* - \widehat{\mathbf{Q}} \right\|_2 \leq O \left( \lambda_{r+1}^* + \frac{\lambda_1^*}{\delta^*} \|\mathbf{H}\|_2 \right).$$

*Proof.* Since  $\mathbf{H}$  is Hermitian, we must have that  $\mathbf{Q}$  is Hermitian. Recall that we defined  $\mathbf{Q}_r^* = \mathbf{U}^* \mathbf{\Lambda} \mathbf{U}^{*\dagger}$  as the top- $r$  eigendecomposition of  $\mathbf{Q}^*$ , where  $\mathbf{U}^* \in \mathbb{C}^{n \times r}$  and  $\mathbf{\Lambda} \in \mathbb{R}^{r \times r}$ . Then we have that

$$\begin{aligned} \left\| \mathbf{Q}^* - \widehat{\mathbf{Q}} \right\|_2 &= \left\| \mathbf{Q}^* - \mathbf{Q} + \mathbf{Q} - \widehat{\mathbf{Q}} \right\|_2 \\ &\leq \left\| \mathbf{Q}^* - \mathbf{Q} \right\|_2 + \left\| \mathbf{Q} - \widehat{\mathbf{Q}} \right\|_2 \\ &= \|\mathbf{H}\|_2 + \left\| \mathbf{Q} - \widehat{\mathbf{Q}} \right\|_2. \end{aligned}$$

We can easily notice that  $\widehat{\mathbf{Q}}$  is the top- $r$  eigendecomposition of  $\mathbf{Q}$ , since  $\mathbf{U} = \mathbf{V}$  due to the fact that  $\mathbf{Q}$  is Hermitian. Therefore, we have that  $\left\| \mathbf{Q} - \widehat{\mathbf{Q}} \right\|_2 = \lambda_{r+1}(\mathbf{Q})$ . By Weyl's inequality, we have that

$$|\lambda_{r+1}(\mathbf{Q}) - \lambda_{r+1}^*| \leq \|\mathbf{H}\|_2.$$

Therefore, we can conclude that  $\lambda_{r+1}(\mathbf{Q}) \leq \lambda_{r+1}^* + \|\mathbf{H}\|_2$ . This gives that

$$\left\| \mathbf{Q} - \widehat{\mathbf{Q}} \right\|_2 \leq \lambda_{r+1}^* + \|\mathbf{H}\|_2,$$

which implies that

$$\left\| \mathbf{Q}^* - \widehat{\mathbf{Q}} \right\|_2 \leq \lambda_{r+1}^* + 2\|\mathbf{H}\|_2 = O(\lambda_{r+1}^* + \|\mathbf{H}\|_2).$$

□

Now, we are ready to prove Corollary D.3.

*Proof of Corollary D.3.* Under the provided condition, we can apply Lemma D.4 to obtain that

$$\left\| \mathbf{Q}^* - \widehat{\mathbf{Q}} \right\|_2 \leq O(\lambda_{r+1}^* + \|\mathbf{H}\|_2).$$

Plugging the bound into Lemma D.1 gives

$$\left| \mathbf{z}^{*\dagger} \mathbf{Q}^* \mathbf{z}^* - \mathbf{z}_r \mathbf{Q}^* \mathbf{z}_r \right| \leq O(n(\lambda_{r+1}^* + \|\mathbf{H}\|_2)).$$

□

## D.4 Extension to complex Gaussian noise

Theorem 4 made no assumptions on the noise matrix  $\mathbf{H}$ . With different assumptions on  $\mathbf{H}$ , we may be able to decrease the bound in Theorem 4. In this section, we give a simple result for  $\mathbf{H}_{i,j} \sim \mathcal{N}_{\mathbb{C}}(0, \varepsilon^2)$  independently by leveraging a result of [BAL19].

**Corollary D.5.** *Let  $\mathbf{z}_r, \text{OPT-}\mathbf{Q}^*$  be defined in (17). Let  $\lambda_j^*$  be the  $j$ th eigenvalue of  $\mathbf{Q}^*$  with  $\lambda_j^* = 0$  if  $j > r$ , and define  $\delta^* = \min \{ \min_{j \in [r-1]} |\lambda_j^* - \lambda_{j+1}^*|, \lambda_r^* \}$ . Let  $\mathbf{H} \in \mathbb{C}^{n \times n}$  such that  $H_{i,k} \sim \mathcal{N}_{\mathbb{C}}(0, \alpha^2)$  for some  $\alpha \in \mathbb{R}$ . If  $\alpha \leq \frac{c\delta^*}{\sqrt{n}}$  for some small enough constant  $c$ , then, there exist constants  $C, c' > 0$  such that with*

probability at least  $1 - C \exp(-c'n)$ , we have that:

$$|\text{OPT}-\mathbf{Q}^* - \mathbf{z}_r \mathbf{Q}^* \mathbf{z}_r| \leq O \left( n \lambda_{r+1}^* + \frac{n^{\frac{3}{2}} \lambda_1^* \varepsilon}{\delta^*} \right).$$

Here, we extend Corollary D.3 by bounding the operator norm of  $\mathbf{H}$  by  $\sqrt{n} \lambda_1^* \varepsilon$ . Note that this bound on the operator norm matches the standard result in the real case [Ver18], both with a scaling of  $\sqrt{n}$ . In addition, Corollary D.5 implies that the noise term dominates only when  $\varepsilon \geq \Omega \left( \frac{\delta^* \lambda_{r+1}^*}{\lambda_1^* \sqrt{n}} \right)$ , showcasing a relationship between the approximation error, the noise scale, and the threshold rank  $r$ .

*Proof of Corollary D.5.* By definition, since  $H_{i,k} \sim \mathcal{N}_{\mathbb{C}}(0, \alpha^2)$ , we have that  $\text{Re}(H_{i,k}), \text{Im}(H_{i,k}) \sim \mathcal{N}\left(0, \frac{\alpha^2}{2}\right)$  independently. Thus, we have that  $H_{i,k}$  is sub-Gaussian in the complex space, which allows us to use Theorem 18 to obtain that, with probability at least  $1 - C \exp(-c'n)$ ,

$$\|\alpha^{-1} \mathbf{H}\|_2 \leq O(\sqrt{n}) \Rightarrow \|\mathbf{H}\|_2 \leq O(\alpha \sqrt{n}).$$

Notice the choice of  $\alpha$ ; plugging that upper bound into (18) gives the desired result.  $\square$

## D.5 Proof of Theorem 5

**Theorem 5.** Let  $\mathbf{Q}^*$  be a rank- $r$  Hermitian matrix. Let  $\mathbf{H} \in \mathbb{C}^{n \times n}$ . Assume we observe  $\mathbf{Q} = \mathbf{Q}^* + \mathbf{H}$ . Let  $\mathbf{z}_r$  be the output of (17) with  $K \geq 3$ . Recall that  $\mathbf{u}_i^*$  is the  $i$ th eigenvector of  $\mathbf{Q}^*$ . If  $\mathbf{Q}^*$  satisfies the incoherence condition  $\|\mathbf{u}_1^*\|_{\infty} \leq \frac{\mu}{\sqrt{n}}$ , where  $\mu$  is some absolute constant, then

$$\frac{\mathbf{z}_r^\dagger \mathbf{Q}^* \mathbf{z}_r}{\text{OPT}-\mathbf{Q}^*} \geq 1 - O \left( \frac{\lambda_{r+1}^*}{\lambda_1^*} + \frac{\|\mathbf{H}\|_2}{\delta^*} \right). \quad (19)$$

*Proof of Theorem 5.* By Theorem 4, we know

$$\mathbf{z}^{*\dagger} \mathbf{Q}^* \mathbf{z}^* - \mathbf{z}_r^\dagger \mathbf{Q}^* \mathbf{z}_r \leq O \left( n \left( \lambda_{r+1}^* + \frac{\lambda_1^*}{\delta^*} \|\mathbf{H}\|_2 \right) \right).$$

We can rearrange this bound to get a bound on the approximation ratio in terms of  $\text{OPT}-\mathbf{Q}^*$  as follows:

$$\frac{\mathbf{z}_r^\dagger \mathbf{Q}^* \mathbf{z}_r}{\text{OPT}-\mathbf{Q}^*} \geq 1 - \frac{O \left( n \left( \lambda_{r+1}^* + \frac{\lambda_1^*}{\delta^*} \|\mathbf{H}\|_2 \right) \right)}{\text{OPT}-\mathbf{Q}^*}. \quad (74)$$

We now focus on lower bounding  $\text{OPT}-\mathbf{Q}^* = \mathbf{z}^{*\dagger} \mathbf{Q}^* \mathbf{z}^*$ . To do so, we introduce  $\hat{\mathbf{z}} \in \mathcal{A}_K^n$ . For now, we can treat  $\hat{\mathbf{z}}$  as an arbitrary vector in  $\mathcal{A}_K^n$ . In Equation (75), we show that we can choose  $\hat{\mathbf{z}}$  to satisfy certain nice properties that allow us to lower bound  $\hat{\mathbf{z}}^\dagger \mathbf{Q}^* \hat{\mathbf{z}}$ .

We can rewrite  $\hat{\mathbf{z}}^\dagger \mathbf{Q}^* \hat{\mathbf{z}}$  in terms of the decomposition of  $\mathbf{Q}^*$  as follows.

$$\begin{aligned} \hat{\mathbf{z}}^\dagger \mathbf{Q}^* \hat{\mathbf{z}} &= \hat{\mathbf{z}}^\dagger \left( \sum_{i=1}^r \lambda_i^* \mathbf{u}_i^* \mathbf{u}_i^{*\dagger} \right) \hat{\mathbf{z}} \\ &= \sum_{i=1}^r \lambda_i^* (\hat{\mathbf{z}}^\dagger \mathbf{u}_i^*) (\mathbf{u}_i^{*\dagger} \hat{\mathbf{z}}) \\ &= \sum_{i=1}^r \lambda_i^* |\hat{\mathbf{z}}^\dagger \mathbf{u}_i^*|^2 \\ &\geq \lambda_1^* \cdot |\hat{\mathbf{z}}^\dagger \mathbf{u}_1^*|^2. \end{aligned}$$

We now focus on bounding  $|\hat{\mathbf{z}}^\dagger \mathbf{u}_1^\star|^2$ :

$$\begin{aligned} |\hat{\mathbf{z}}^\dagger \mathbf{u}_1^\star|^2 &= \operatorname{Re}(\hat{\mathbf{z}}^\dagger \mathbf{u}_1^\star)^2 + \operatorname{Im}(\hat{\mathbf{z}}^\dagger \mathbf{u}_1^\star)^2 \\ &= \left[ \operatorname{Re} \left( \sum_{\ell=1}^n \bar{z}_\ell u_{1,\ell}^\star \right) \right]^2 + \left[ \operatorname{Im} \left( \sum_{\ell=1}^n \bar{z}_\ell u_{1,\ell}^\star \right) \right]^2 \\ &= \left[ \sum_{\ell=1}^n \operatorname{Re}(\bar{z}_\ell u_{1,\ell}^\star) \right]^2 + \left[ \sum_{\ell=1}^n \operatorname{Im}(\bar{z}_\ell u_{1,\ell}^\star) \right]^2. \end{aligned}$$

Each entry  $u_{1,\ell}^\star$  of  $\mathbf{u}_1^\star$  may be written in polar form as

$$u_{1,\ell}^\star = r_\ell \exp(j\theta_\ell),$$

where  $r_\ell = |u_{1,\ell}^\star| \in \mathbb{R}$  and  $\theta_\ell \in [0, 2\pi)$ . Additionally, because  $\hat{\mathbf{z}} \in \mathcal{A}_K^n$ ,  $z_\ell^\star = \exp(jk_\ell\pi/K)$  for some  $k_\ell \in \{0, 1, \dots, K-1\}$ . We can re-express the quantity under consideration as:

$$\begin{aligned} |\hat{\mathbf{z}}^\dagger \mathbf{u}_1^\star|^2 &= \left[ \sum_{\ell=1}^n r_\ell \operatorname{Re} \left( \exp \left( j \left( \theta_\ell - \frac{2k_\ell\pi}{K} \right) \right) \right) \right]^2 \\ &\quad + \left[ \sum_{\ell=1}^n r_\ell \operatorname{Im} \left( \exp \left( j \left( \theta_\ell - \frac{2k_\ell\pi}{K} \right) \right) \right) \right]^2 \\ &= \left[ \sum_{\ell=1}^n r_\ell \cos \left( \theta_\ell - \frac{2k_\ell\pi}{K} \right) \right]^2 \\ &\quad + \left[ \sum_{\ell=1}^n r_\ell \sin \left( \theta_\ell - \frac{2k_\ell\pi}{K} \right) \right]^2. \end{aligned}$$

Now, define  $k_\ell \in \{0, \dots, K-1\}$  to be the unique integer such that  $\theta_\ell$  lies in the  $k_\ell$ -th sector:

$$\theta_\ell \in \left[ \frac{(2k_\ell - 1)\pi}{K}, \frac{(2k_\ell + 1)\pi}{K} \right) \pmod{2\pi}. \quad (75)$$

Let  $\theta'_\ell = (\theta_\ell - \frac{2k_\ell\pi}{K}) \pmod{2\pi}$ . By the definition of  $k_\ell$ , we ensure that the rotated angle is close to zero, specifically  $\theta'_\ell \in [0, \frac{\pi}{K}) \cup [\frac{(2K-1)\pi}{K}, 2\pi)$  for all  $\ell \in [n]$ . Consequently, the cosine of the offset angle is bounded below by the cosine of the maximum deviation  $\pi/K$ :

$$\cos \left( \theta_\ell - \frac{2k_\ell\pi}{K} \right) \in \left[ \cos \left( \frac{\pi}{K} \right), 1 \right].$$

This implies that

$$|\hat{\mathbf{z}}^\dagger \mathbf{u}_1^\star|^2 \geq \left( \sum_{\ell=1}^n r_\ell \cos \left( \frac{\pi}{K} \right) \right)^2 = \cos^2 \left( \frac{\pi}{K} \right) \|\mathbf{u}_1^\star\|_1^2 \geq \frac{1}{4} \|\mathbf{u}_1^\star\|_1^2,$$

where the final inequality holds for all  $K \geq 3$ . In order to lower bound  $\|\mathbf{u}_1^\star\|_1$ , we notice that

$$1 = \|\mathbf{u}_1^\star\|_2^2 \leq \|\mathbf{u}_1^\star\|_1 \|\mathbf{u}_1^\star\|_\infty$$

By the assumption that  $\|\mathbf{u}_1^*\|_\infty \leq \frac{\mu}{\sqrt{n}}$ , we have that

$$\|\mathbf{u}_1^*\|_1 \geq \frac{1}{\|\mathbf{u}_1^*\|_\infty} \geq \frac{\sqrt{n}}{\mu}$$

Ultimately, we have shown that

$$\hat{\mathbf{z}}^\dagger \mathbf{Q}^* \hat{\mathbf{z}} \geq \frac{1n}{4\mu^2} \lambda_1^*.$$

Because  $\mathbf{z}^*$  maximizes  $\mathbf{z}^\dagger \mathbf{Q}^* \mathbf{z}$ , we know

$$\mathbf{z}^{*\dagger} \mathbf{Q}^* \mathbf{z}^* \geq \hat{\mathbf{z}}^\dagger \mathbf{Q}^* \hat{\mathbf{z}}.$$

This allows us to bound  $\text{OPT}-\mathbf{Q}^*$  as follows:

$$\text{OPT}-\mathbf{Q}^* = \mathbf{z}^{*\dagger} \mathbf{Q}^* \mathbf{z}^* \geq \frac{\lambda_1^* n}{4\mu^2}.$$

Substituting this bound back into (74) yields

$$\begin{aligned} \frac{\mathbf{z}_r^\dagger \mathbf{Q}^* \mathbf{z}_r}{\text{OPT}-\mathbf{Q}^*} &\geq 1 - \frac{O\left(n\left(\lambda_{r+1}^* + \frac{\lambda_1^*}{\delta^*} \|\mathbf{H}\|_2\right)\right)}{\lambda_1^* n} \\ &\geq 1 - O\left(\frac{\lambda_{r+1}^*}{\lambda_1^*} + \frac{\|\mathbf{H}\|_2}{\delta^*}\right). \end{aligned}$$

□

## E Experimental Details

### E.1 Experimental Setup.

*Graph Families.* We conduct experiments on three families of graphs: (i)  $\mathcal{G}(n, p)$  (Erdős-Rényi) random graphs with  $n = 20, 50$ , and  $100$ , and  $p = 0.1, 0.25, 0.5, 0.75$  and  $0.9$ ; (ii) Random  $d$ -regular graphs on  $n = 20, 50$  and  $100$  nodes, with  $d = 3, 4$  and  $5$ ; (iii) All GSet benchmark instances [Ye03]. GSet is a benchmark commonly used to evaluate MAX-K-CUT algorithms that consists of 71 graphs ranging in size from 800 to 20,000 nodes. Each GSet graph falls into one of the following categories [DH11]:

1. Erdos-Renyi graphs with edge probability at most 0.03,
2. 2-D toroidal, 4-regular graphs,
3. random graphs with skewed degree distributions.

These graphs either have binary (0 or 1) edge weights or have edge weights in  $\{-1, 0, +1\}$ .

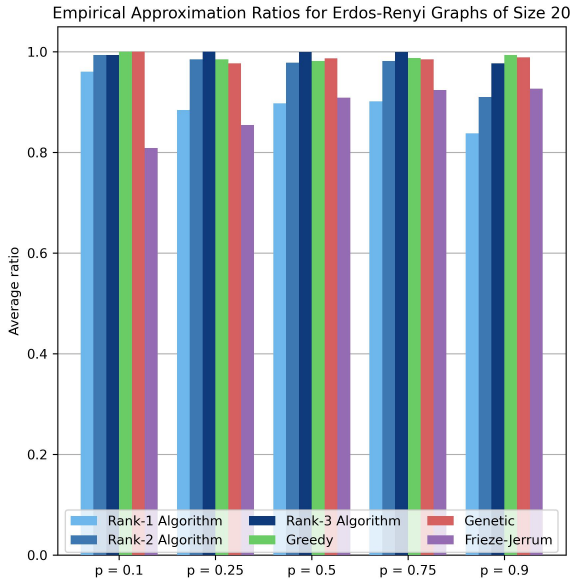
*Baseline Algorithms.* We compare our algorithms to the following baselines: (i) FRIEZE-JERRUM [FJ97]: an SDP relaxation and rounding scheme; (ii) GREEDY [GJG18]: a greedy algorithm that iteratively identifies and locks the single-best node assignment; (iii) GENETIC [PJ16]: a genetic algorithm that maintains a set of candidate cuts and iteratively selects the best of this set, mixes pairs of cuts, and randomly perturbs the worst. On the GSet benchmark, we also compare to a random baseline, RANDOM. To ensure a fair comparison to RANK-1, RANDOM generates  $n + 1$  random cuts and selects the best one, matching the number of candidate solutions enumerated by our algorithm.

*Implementation Details.* All experiments were conducted on HPE ProLiant DL360 Gen11 compute nodes (Sapphire Rapids) equipped with Intel Xeon Platinum 8468 CPUs (96 cores at 2.10 GHz). We generate 20 instances for each size and parameter of the small random graphs using the NetworkX library [HSS08] with fixed random seeds. We use the implementation of [QXW<sup>+</sup>24] for the GREEDY and GENETIC algorithms. We institute a 30-minute timeout limit for all experiments.

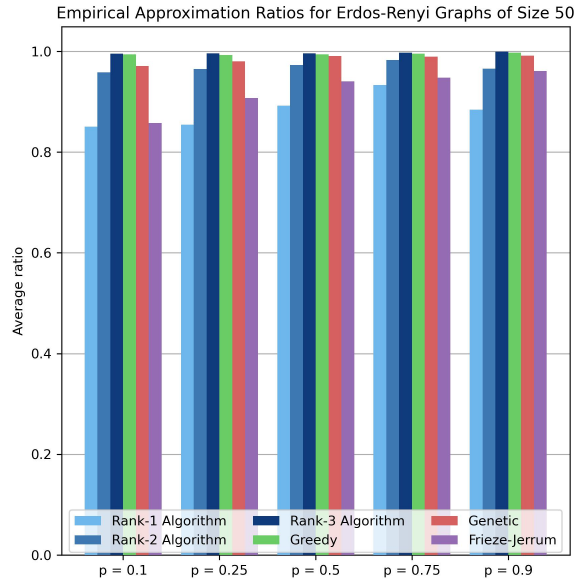
*Evaluation Metrics.* To measure the quality of the MAX-3-CUT approximations found by each algorithm on random graphs, we calculate the ratio of its score to the best score found by any algorithm. We report the average ratio across all random seeds.

## E.2 Experiments on Small Graphs

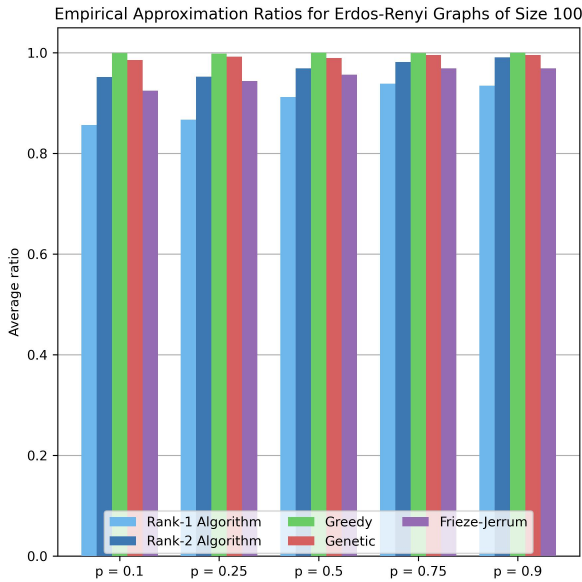
Figures 3 and 4 provide additional results on small, synthetic graph instances.



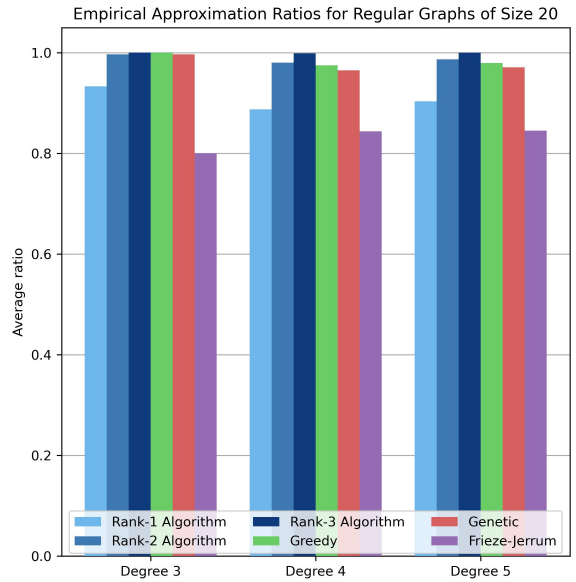
(a) Empirical approximation ratios on Erdős-Rényi graphs with  $n = 20$  nodes.



(b) Empirical approximation ratios on Erdős-Rényi graphs with  $n = 50$  nodes.

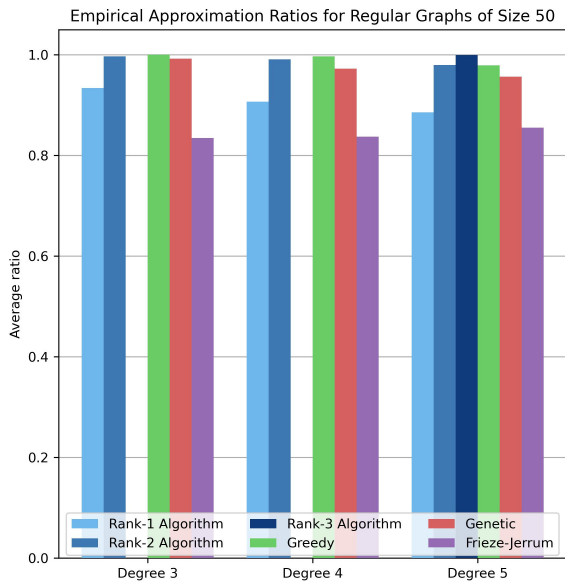


(c) Empirical approximation ratios on Erdős-Rényi graphs with  $n = 100$  nodes. This chart matches the right-hand sub-figure of Figure 2.

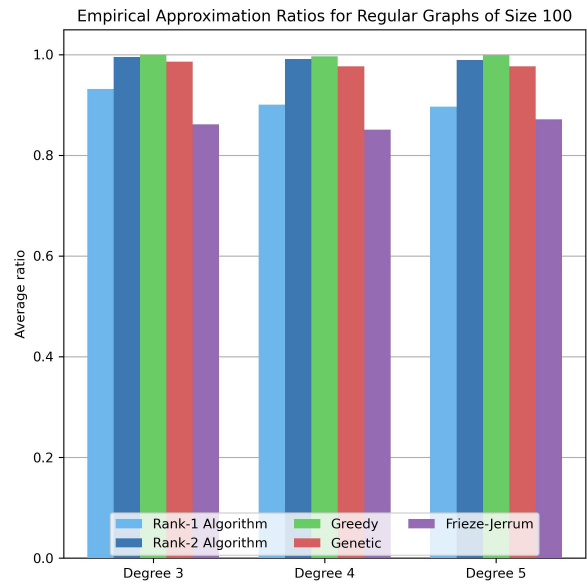


(d) Empirical approximation ratios on regular graphs with  $n = 20$  nodes.

Figure 3



(a) Empirical approximation ratios on regular graphs with  $n = 50$  nodes.



(b) Empirical approximation ratios on regular graphs with  $n = 100$  nodes.

Figure 4

Table 3

Instance	$n$	Type	Binary	RANDOM	GREEDY	GENETIC	MOH	RANK-1
G1	800	Erdos-Renyi	Yes	13024 (0.45s)	14859 (16.3s)	14087 (1083s)	15165	13331 (1.08s)
G2	800	Erdos-Renyi	Yes	12957 (0.44s)	14790 (16.3s)	13992 (1078s)	15172	13291 (1.06s)
G3	800	Erdos-Renyi	Yes	12978 (0.44s)	14795 (16.3s)	14019 (1077s)	15173	13299 (1.06s)
G4	800	Erdos-Renyi	Yes	12998 (0.44s)	14806 (9.9s)	14041 (1080s)	15184	13316 (1.05s)
G5	800	Erdos-Renyi	Yes	13010 (0.44s)	14835 (11.5s)	14060 (1078s)	15193	13334 (1.05s)
G6	800	Erdos-Renyi	No	94 (0.23s)	2082 (11.4s)	1223 (936s)	2632	992 (0.64s)
G7	800	Erdos-Renyi	No	112 (0.23s)	2082 (11.4s)	1223 (936s)	2409	992 (0.64s)
G8	800	Erdos-Renyi	No	99 (0.23s)	2079 (11.4s)	1226 (935s)	2428	989 (0.63s)
G9	800	Erdos-Renyi	No	103 (0.22s)	2076 (11.4s)	1224 (934s)	2478	991 (0.64s)
G10	800	Erdos-Renyi	No	95 (0.22s)	2076 (11.4s)	1223 (934s)	2407	992 (0.64s)
G11	800	Toroidal	No	95 (0.22s)	619 (11.5s)	406 (1075s)	669	426 (0.51s)
G12	800	Toroidal	No	92 (0.22s)	618 (11.5s)	405 (1075s)	660	425 (0.50s)
G13	800	Toroidal	No	90 (0.22s)	617 (11.5s)	404 (1075s)	686	424 (0.50s)
G14	800	Skew	Yes	3224 (0.23s)	3914 (11.5s)	3665 (1166s)	4012	3217 (0.56s)
G15	800	Skew	Yes	3223 (0.23s)	3911 (11.5s)	3663 (1166s)	3984	3215 (0.56s)
G16	800	Skew	Yes	3223 (0.23s)	3910 (11.5s)	3663 (1166s)	3991	3214 (0.56s)
G17	800	Skew	Yes	3221 (0.23s)	3909 (11.5s)	3662 (1166s)	3983	3213 (0.56s)
G18	800	Skew	No	38 (0.22s)	952 (11.4s)	584 (1169s)	1207	483 (0.49s)
G19	800	Skew	No	39 (0.22s)	952 (11.4s)	584 (1169s)	1081	483 (0.49s)
G20	800	Skew	No	39 (0.22s)	952 (11.4s)	584 (1169s)	1122	483 (0.49s)
G21	800	Skew	No	39 (0.22s)	952 (11.4s)	584 (1169s)	1109	483 (0.49s)

Table 4

Instance	$n$	Type	Binary	RANDOM	GREEDY	GENETIC	MOH	RANK-1
G22	2,000	Erdos-Renyi	Yes	26434 (2.45s)	30400 (111.1s)	29043 (1092s)	17167	27385 (5.50s)
G23	2,000	Erdos-Renyi	Yes	26406 (2.45s)	30369 (111.1s)	29022 (1090s)	17168	27363 (5.50s)
G24	2,000	Erdos-Renyi	Yes	26403 (2.45s)	30352 (111.1s)	29011 (1090s)	17162	27350 (5.49s)
G25	2,000	Erdos-Renyi	Yes	26396 (2.45s)	30350 (111.1s)	29007 (1089s)	17163	27348 (5.50s)
G26	2,000	Erdos-Renyi	Yes	26433 (2.45s)	30393 (111.1s)	29038 (1090s)	17154	27379 (5.49s)
G27	2,000	Erdos-Renyi	No	190 (1.22s)	5366 (100.5s)	3703 (953s)	4020	2894 (1.36s)
G28	2,000	Erdos-Renyi	No	211 (1.22s)	5350 (100.5s)	3704 (953s)	3973	2907 (1.36s)
G29	2,000	Erdos-Renyi	No	202 (1.22s)	5347 (100.5s)	3703 (953s)	4106	2905 (1.36s)
G30	2,000	Erdos-Renyi	No	197 (1.22s)	5343 (100.5s)	3703 (953s)	4119	2902 (1.36s)
G31	2,000	Erdos-Renyi	No	205 (1.22s)	5333 (100.5s)	3700 (953s)	4003	2901 (1.36s)
G32	2,000	Toroidal	No	202 (1.19s)	1486 (100.5s)	1048 (1104s)	1653	1205 (1.27s)
G33	2,000	Toroidal	No	204 (1.19s)	1484 (100.5s)	1047 (1104s)	1625	1204 (1.27s)
G34	2,000	Toroidal	No	202 (1.19s)	1484 (100.5s)	1047 (1104s)	1607	1204 (1.27s)
G35	2,000	Skew	Yes	8008 (1.25s)	8897 (101.5s)	8591 (1193s)	10046	8038 (1.36s)
G36	2,000	Skew	Yes	8010 (1.25s)	8898 (101.5s)	8592 (1193s)	10039	8038 (1.36s)
G37	2,000	Skew	Yes	8010 (1.25s)	8898 (101.5s)	8592 (1193s)	10052	8038 (1.36s)
G38	2,000	Skew	Yes	8010 (1.25s)	8898 (101.5s)	8592 (1193s)	10040	8038 (1.36s)
G39	2,000	Skew	No	138 (1.14s)	3005 (101.5s)	2211 (1203s)	2903	1773 (1.29s)
G40	2,000	Skew	No	137 (1.14s)	3002 (101.5s)	2210 (1203s)	2870	1771 (1.29s)
G41	2,000	Skew	No	140 (1.14s)	3000 (101.5s)	2210 (1203s)	2887	1771 (1.29s)
G42	2,000	Skew	No	139 (1.14s)	3001 (101.5s)	2210 (1203s)	2980	1770 (1.29s)

Table 5

Instance	$n$	Type	Binary	RANDOM	GREEDY	GENETIC	MOH	RANK-1
G43	1,000	Erdos-Renyi	Yes	16062 (1.08s)	18616 (47.8s)	17577 (1088s)	8578	16511 (2.05s)
G44	1,000	Erdos-Renyi	Yes	16060 (1.08s)	18599 (47.8s)	17565 (1088s)	8571	16500 (2.05s)
G45	1,000	Erdos-Renyi	Yes	16054 (1.08s)	18599 (47.8s)	17565 (1088s)	8568	16501 (2.05s)
G46	1,000	Erdos-Renyi	Yes	16052 (1.08s)	18604 (47.8s)	17568 (1088s)	8568	16504 (2.05s)
G47	1,000	Erdos-Renyi	Yes	16050 (1.08s)	18600 (47.8s)	17566 (1088s)	8572	16501 (2.05s)
G48	3,000	Toroidal	Yes	4108 (4.3s)	5998 (299s)	—	6000	6000 (5.2s)
G49	3,000	Toroidal	Yes	4150 (4.3s)	5996 (394s)	—	6000	6000 (5.2s)
G50	3,000	Toroidal	Yes	4132 (4.3s)	5998 (399s)	—	6000	5934 (6.0s)
G51	1,000	Skew	Yes	3847 (1.09s)	4555 (48.1s)	4284 (1172s)	5037	3898 (1.24s)
G52	1,000	Skew	Yes	3847 (1.09s)	4555 (48.1s)	4284 (1172s)	5040	3898 (1.24s)
G53	1,000	Skew	Yes	3847 (1.09s)	4555 (48.1s)	4284 (1172s)	5039	3898 (1.24s)
G54	1,000	Skew	Yes	3847 (1.09s)	4555 (48.1s)	4284 (1172s)	5036	3898 (1.24s)
G55	5,000	Erdos-Renyi	Yes	49385 (20.7s)	54577 (934s)	—	12429	50996 (64.9s)
G56	5,000	Erdos-Renyi	No	347 (8.71s)	12498 (940s)	—	4752	6794 (10.4s)
G57	5,000	Toroidal	No	350 (8.72s)	3781 (940s)	—	4083	3912 (10.4s)
G58	5,000	Skew	Yes	10057 (9.23s)	11696 (940s)	—	25195	10232 (10.4s)
G59	5,000	Skew	No	249 (8.67s)	3762 (940s)	—	7262	2928 (10.4s)

Table 6

Instance	$n$	Type	Binary	RANDOM	GREEDY	GENETIC	MOH	RANK-1
G60	7,000	Erdos-Renyi	Yes	87633 (52.4s)	95057 (2583s)	—	17076	89341 (207s)
G61	7,000	Erdos-Renyi	No	463 (22.1s)	18612 (2603s)	—	6853	8734 (25.9s)
G62	7,000	Toroidal	No	452 (22.1s)	6198 (2603s)	—	5685	5785 (25.8s)
G63	7,000	Skew	Yes	19212 (24.4s)	22675 (2605s)	—	15322	19507 (27.5s)
G64	7,000	Skew	No	381 (22.0s)	8938 (2614s)	—	10443	5620 (25.8s)
G65	8,000	Toroidal	No	557 (28.9s)	7417 (2936s)	—	6490	6806 (33.7s)
G66	9,000	Toroidal	No	584 (36.5s)	7482 (3308s)	—	7416	7781 (41.4s)
G67	10,000	Toroidal	No	147 (49s)	—	—	8086	3117 (57s)
G70	10,000	Erdos-Renyi	Yes	9333 (50.6s)	—	—	9999	6832 (56.6s)
G72	10,000	Toroidal	No	217 (48.7s)	—	—	8192	3849 (56.6s)
G77	14,000	Toroidal	No	795 (134s)	—	—	11578	5118 (145s)
G81	20,000	Toroidal	No	1135 (272s)	—	—	16321	5541 (280s)